Materials Today Energy 5 (2017) 22–36

Contents lists available at ScienceDirect

Materials Today Energy

journal homepage: www.journals.elsevier.com/materials-today-energy/

Two-dimensional MXenes for energy storage and conversion applications

Yijing Sun, Dongsheng Chen, Ziqi Liang*

Department of Materials Science, Fudan University, Shanghai 200433, China

ARTICLE INFO

Article history:
Received 6 March 2017
Received in revised form
10 April 2017
Accepted 29 April 2017

Keywords:
Two-dimensional
MXenes
Supercapacitor
Battery
Thermoelectric applications

ABSTRACT

An emerging family of layered early transition metal carbides and/or nitrides—MXenes—has been intensively investigated by both theoretical calculations and experimental research to explore their unique properties and potential applications. The two-dimensional film morphology coupled with a fascinating combination of metallic conductivity and the hydrophilic nature of their functionalized surface render them as promising candidates for a wide range of utilizations. This article reviews recent advances on MXenes and their composites with either polymers or small molecules. Their wet chemistry and structural characterization are first described. Then we discuss in detail their numerous applications of energy storage and conversion including supercapacitors, batteries and thermoelectric devices. In particular, their electrochemical and thermoelectric properties, performances and mechanisms are presented with regard to their respective structures, compositions and fabrication methods. Finally, a conclusion of recent progress on MXenes is made with a perspective for their possible future directions.

1. Introduction

Two-dimensional (2D) materials have obtained increasing research attention due to their remarkable electrical and electronic properties that are distinct from their bulk counterparts. The most studied 2D material is graphene, which exhibits high intrinsic mobility, good electrical conductivity and excellent mechanical stability, thus enabling a wide range of applications from flexible electronics, field-effect transistors to energy conversion and storage devices [1,2]. Other 2D materials beyond graphene, such as transition metal dichalcogenides (TMDs), hexagonal boron nitride, metal oxide and hydroxides, have been extensively explored over the past several years [3–8].

Recently, an emerging family of 2D early transition metal carbides and/or nitrides termed as MXenes was discovered by the Gogotsi group at Drexel University, USA [9]. They are generally produced through selective extraction of the A-layers from the layered hexagonal $M_{n+1}AX_n$ or MAX phases, where M is an early transition metal such as Ti, V, Nb and Ta, A is mainly a group 13 or 14 element such as Al and Si, X is C and/or N, and n = 1, 2, or 3 [10]. The MXenes can be more accurately referred as $M_{n+1}X_nT_x$ in which T_x represents the functional termination groups—generally O, OH and F. By far, more than a dozen MXenes have been experimentally synthesized including $Ti_3C_2T_x$, Ti_2CT_x, $TiNbCT_x$, Ti_3CNT_x, $Ti_4N_3T_x$, V_2CT_x, Nb_2CT_x, $Nb_4C_3T_x$, Mo_2CT_x, $Zr_3C_2T_x$, $Ta_4C_3T_x$, $(Ti_{0.5}, Nb_{0.5})_2CT_x$, $(V_{0.5}, Cr_{0.5})_3C_2T_x$, $(Nb_{0.8}Ti_{0.2})_4C_3T_x$, and $(Nb_{0.8}Zr_{0.2})_4C_3T_x$ [9–18]. MXenes that are composed of other M element such as Sc and Hf have also been predicted via density functional theory (DFT) [19]. In addition, Anasori et al. theoretically indicated the existence and stability of new, ordered double-MXenes, viz. $M'_2M''C_2$ and $M'_2M''_2C_2$, where M″-layer is sandwiched between outer M′C layers [12]. They also synthesized such double-MXenes as Mo_2TiC_2, $Mo_2Ti_2C_3$ and Cr_2TiC_2, which further enriches these emerging 2D materials.

Researchers have carried out intensive computational modeling and simulation to understand the structure of MXenes and predict their properties, both of which are further experimentally investigated in details [10,20–22]. As shown in Fig. 1a, in a general atomistic model for MXenes, the M atoms are arranged on the lattice point of hexagonal close packing (hcp) while the X atoms occupy the octahedral interstices, which is similar to the MAX parent phase [21]. The attachment of termination groups that are bonded with the surface M atoms stabilizes these close packed MXene sheets [21]. Besides, the surface structure is of critical importance for prediction and manipulation of their properties and applications. In a significantly improved model (see Fig. 1b, c and d),

* Corresponding author.
E-mail address: zqliang@fudan.edu.cn (Z. Liang).

http://dx.doi.org/10.1016/j.mtener.2017.04.008
2468-6069/

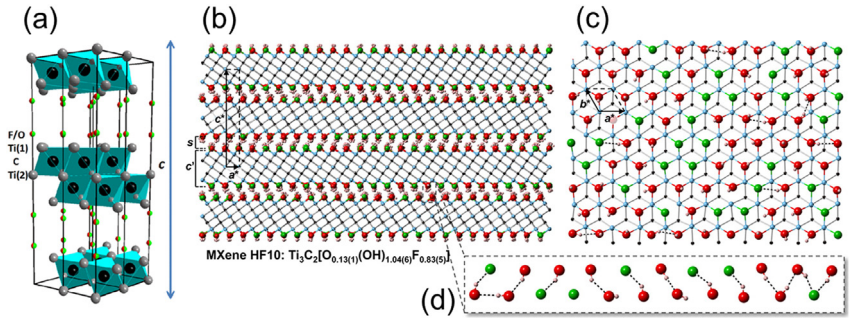

Fig. 1. (a) The polyhedral illustration of optimized $Ti_3C_2T_x$ structure. Ti, C, O, and F atoms are in grey, black, red and green colors. Reproduced with permission from Ref. [21]. Copyright 2014, American Physical Society. Structure representation of MXenes: (b) The stacking direction view. (c) Top view of a single sheet, showing the random occupation of termination groups. (d) The formation of interlayer attractive force. Ti, C, H, O, and F are in blue, black, pink, red and green colors. Reproduced with permission from Ref. [22]. Copyright 2015, American Chemical Society. (For interpretation of the references to colour in this figure legend, the reader is referred to the web version of this article.)

an unprecedentedly detailed structure is experimentally proposed, showing the random and coexisting surface termination groups of a specific MXene sample, which can be extended to simulate other MXene structures and largely increase the accuracy of predicting potential properties [22]. Based on their distinctive structures, MXenes have been predicated to be a host for 2D morphology, inherently high metallic conductivity [23,24], tunable surface functional groups [19,25], excellent mechanical stability [26] and intercalation ability [27–29]. Such compelling characteristics render them promising candidates for numerous electronic applications. These MXenes have exhibited fascinating performance in supercapacitors, batteries and fuel cells [30–33]. MXenes can be also applied in other fields including waste treatment [34,35], water purification [36,37], chemical sensors [38] and catalysts [39,40].

In this review, we aim to present recent advances in this emerging MXenes for energy storage and conversion applications. The solution chemistry of MXenes is first described and related structural characterization methods are shown. Then we discuss MXene-based electrodes in supercapacitors and several types of batteries, followed by the thermoelectric properties of MXenes. Finally, a conclusion of the research on MXenes is given and a perspective for future direction is offered.

2. Synthesis and characterization

In contrast to the weak van der Waals interactions between the layers of graphite, the strong M–X bonds and M–A bonds in MAX phases can hardly be broken by mechanical ways. However, by taking the differences of relative strengths of these bonds into account, the A element can be extracted through chemical methods. For instance, selective removal of A-layers occurs at elevated temperature, yet the structural transformation such as the formation of three-dimensional rock salt is inevitable [41]. Chlorination at high temperature induces the loss of A-layers as well as M element due to the strong activity of Cl_2, forming carbide derived carbons (CDCs) [42].

A delicate balance of the etching ability of etchants and temperature was first achieved by Gogotsi and coworkers, that is, selective etching with aqueous hydrofluoric acid (HF) at room temperature (RT) were managed to synthesize multi-layered MXenes, which not only protects the 2D morphology of MXenes but also permits the complete separation of the A-layers from the MAX parent phase [9]. Specifically, Ti_3AlC_2 powder was immersed and stirred in 50% concentrated aqueous HF at RT for 2 h, followed by washing several times with deionized water to remove the by-products (see Fig. 2a and b) [9]. The above-mentioned reaction between Ti_3AlC_2 and HF can be simplified as the following equations:

$$Ti_3AlC_2 + 3HF = AlF_3 + 3/2H_2 + Ti_3C_2 \quad (1)$$

$$Ti_3C_2 + 2H_2O = Ti_3C_2(OH)_2 + H_2 \quad (2)$$

$$Ti_3C_2 + 2HF = Ti_3C_2F_2 + H_2 \quad (3)$$

Equation (1) is the essential reaction, followed by equation (2) and/or (3), which is an indicator for the formation of terminal surface instead of bare MXenes [9]. This simple method can be extended to fabricate other MXenes, such as Ti_2C, Ta_4C_3, $(Ti_{0.5}, Nb_{0.5})_2C$, $(V_{0.5}, Cr_{0.5})_3C_2$, Ti_3CN, Mo_2TiC_2, $Mo_2Ti_2C_3$ and Cr_2TiC_2 [12,13]. However, only the MAX phase, where the A element is Al, can be etched by HF and then exfoliated into MXenes [43]. Interestingly, Zhou and co-workers have successfully obtained first 2D $Zr_3C_2T_x$ by selective etching of Al_3C_3 from an alternative layered ternary $Zr_3Al_3C_5$ beyond MAX phase, which opens up a new way to synthesis Zr- and even Hf-containing MXenes [11]. To acquire single or few-layered MXenes, either dimethyl sulphoxide (DMSO) [27] or iso-propylamine [44] were intercalated into these sheets, followed by sonication treatment in water.

It is noteworthy that several etching conditions including etching time, HF concentration, MAX particle size and reaction temperature play critical roles on the conversion of MAX phase to MXene. To form different MXenes from corresponding MAX parent phase at RT required varying HF concentrations and etching time. For instance, a prolongation of etching time can result in the holes in $Ta_4C_3T_x$ [13]. Decreasing the MAX particle size via ball-milling or attrition effectively reduced the etching time from ~90 h to 8 h for the formation of V_2CT_x [14]. Stirring Ti_2AlC powders in the same concentrated HF that is used to treat Ti_3AlC_2 caused their complete dissolution and therefore the HF concentration should decrease to 10% to produce Ti_2C from Ti_2AlC phase [13]. Besides, the proportions of the surface termination groups were highly dependent on the reaction conditions [45].

Despite the achieved success on producing MXenes in HF solutions, both the toxicity of HF and restriction on specific MAX phase hinder the further development and application of this method to fabricate desired MXene sheets. Hence, other milder and less hazardous etchants have been explored [20,23,24,46,47]. Halim et al. reported on a new etchant ammonium bifluoride (NH_4HF_2) to etch epitaxial Ti_3AlC_2, which simultaneously led to an intercalation of NH_3 and NH_4^+ into the interlayers of $Ti_3C_2T_x$ and an increase of

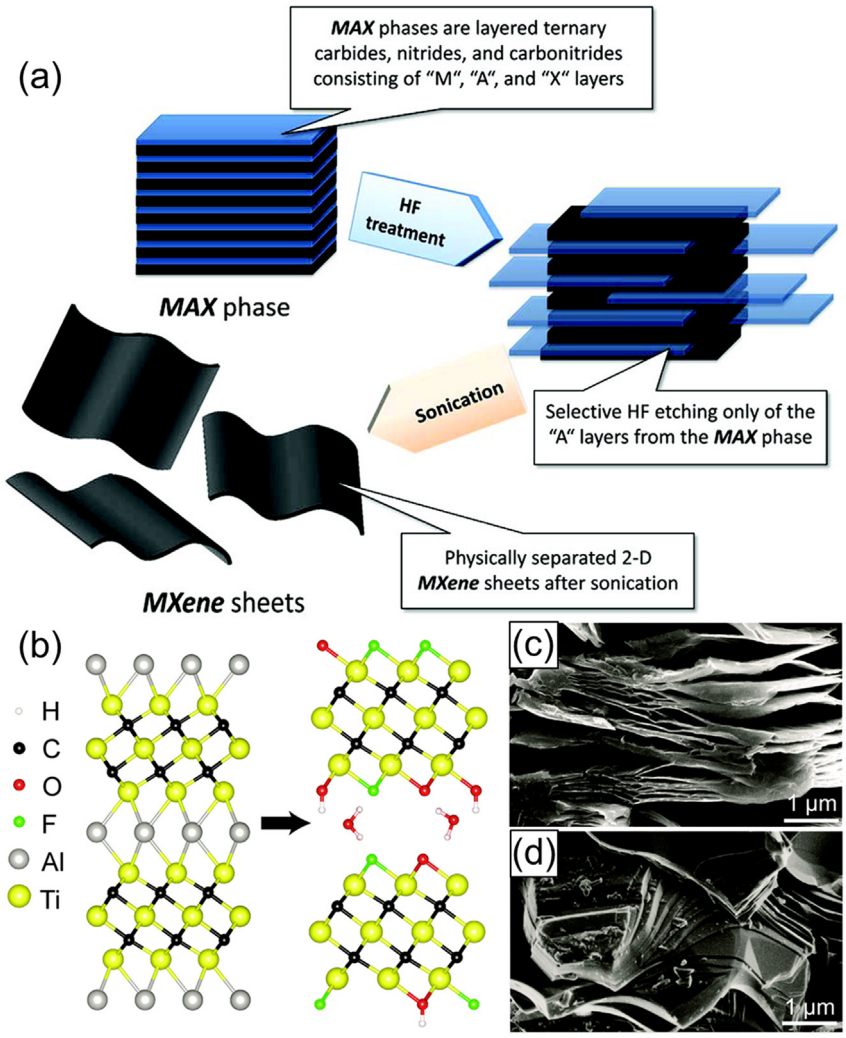

Fig. 2. (a) Schematic illustration of the exfoliation process for MXenes. Reproduced with permission from Ref. [13]. Copyright 2012, American Chemical Society. (b) Schematic of etching from MAX phase to MXene showing terminations and adsorbed water. SEM image of (c) HF-etched MXene and (d) LiF + HCl etched MXene. Reproduced with permission from Ref. [45]. Copyright 2016, Royal Society of Chemistry.

the c lattice parameters [24]. Ghidiu et al. showed a simple and scalable alternative method to fabricate $Ti_3C_2T_x$ 'clay' distinct from previous laborious technique. According to their synthesis route, Ti_3AlC_2 powders were slowly added into a mixed solution of hydrochloric acid (HCl) and lithium fluoride (LiF), which was heated to 40 °C for 45 h and then washed to remove the reaction by-products, yielding clay-like sediments [23]. The resulting MXenes exhibited more compact structures without visible delamination, while the HF-etched Ti_3AlC_2 appeared accordion-like morphology (see Fig. 2c and d) [45]. The Ti vacancy concentration and defects can be controlled though the etchant concentration during LiF and HCl treatment [48]. Apart from the above noted NH_4HF_2 and LiF, other fluoride salts including alkali metal fluoride, calcium fluoride (CaF_2) and tetrabutylammonium fluoride have been used to replace NH_4HF_2 and LiF to form the etching solution with either HCl or H_2SO_4 [20].

Hydrothermal synthesis is also an effective means of producing multi-layered MXenes. For example, Xie et al. introduced a novel method to leach the Al-layers from MAX phase via a H_2SO_4 hydrothermal treatment of Ti_3AlC_2 with NaOH solution at 80 °C [49]. Wang et al. produced $Ti_3C_2T_x$ by immersing Ti_3AlC_2 powders in aqueous NH_4F, followed by a hydrothermal reaction of this mixture [50].

Except for the substitution of dangerous etchants, a new solid solution based exfoliation approach without etchant has been demonstrated by Zhang and co-workers. They indicated that only doped MAX phase, such as $Ti_3Si_{0.75}Al_{0.25}C_2$, can be exfoliated in various solvents by ultrasonication, yet the yield was relatively low and as-prepared MXenes nanosheets contained a small amount of TiC [43].

X-ray diffraction (XRD) patterns offer adequate information to determine whether a MAX phase is transformed to MXene or not. After transformation to MXenes, all of characteristic peaks except the (000l) band are weakened or vanish. Besides, the (000l) peaks are broadened and shift to lower angles, indicating the change of c lattice parameter [9]. As shown in Fig. 3a, when the MAX phase was treated by HF, a significant weakening of the peaks was observed and an amorphous broad peak appeared. After exfoliation, the (000l) peaks became broad and shifted to lower angles [14]. However, XRD patterns of the $Ti_3C_2T_x$ that was etched by the

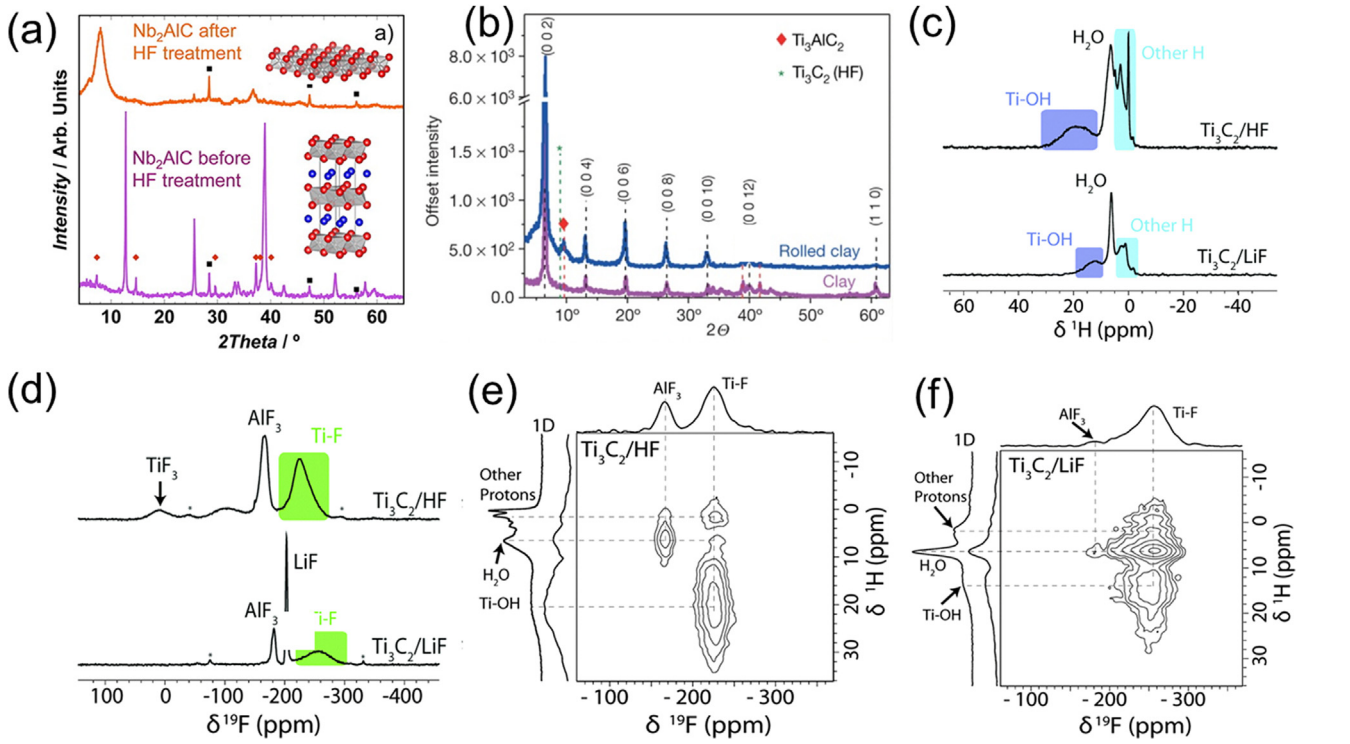

Fig. 3. (a) XRD patterns of Nb_2AlC and Nb_2CT_x treated by HF. Reproduced with permission from Ref. [14]. Copyright 2013, American Chemical Society. (b) XRD patterns for $Ti_3C_2T_x$ treated by LiF + HCl etching solution. Reproduced with permission from Ref. [23]. Copyright 2014, Nature Publishing Group. (c) ^1H NMR spectra of HF and LiF + HCl synthesized MXene. (d) ^{19}F NMR spectra of HF and LiF + HCl synthesized MXene. ^1H–^{19}F HETCOR NMR spectra of (e) HF and (f) LiF + HCl produced MXene. Reproduced with permission from Ref. [45]. Copyright 2016, Royal Society of Chemistry.

mixture of LiF with HCl exhibited an increase in both the intensity and sharpness (see Fig. 3b), which is different from the broad peaks observed in HF-etched MXenes. This accounts for the intercalation of water and other possible cations into the multiple layers of MXenes [23]. It is worth noting that the fraction of unreacted MAX cannot be quantified by the XRD patterns alone, and the energy-dispersive X-ray spectroscopy (EDS) was thus combined to measure the A:M atomic ratio to estimate the residual MAX phase [10].

X-ray photoelectron spectroscopy (XPS) as well as EDS have been employed to characterize the surface terminations of MXenes. The EDS characterization can quantify their proportions, yet the signal of −O and −OH is difficult to distinguish due to the presence of by-products and adsorbed water [23]. By contrast, the XPS experiments reveal surface elemental compositions more effectively [51].

Recently, nuclear magnetic resonance (NMR) spectroscopy were applied to precisely investigate the surface functionalization of $Ti_3C_2T_x$ and V_2CT_x, especially −H and −F terminations owing to the high sensitivity of ^1H and ^{19}F NMR spectra, which provide deeper insights into not only the proportion of the surface termination groups but also their connectivity in the MXenes [45,52]. For example, Hope et al. found that the $Ti_3C_2T_x$ produced by either HF or LiF + HCl treatment showed a broad signal at 18.6 ppm and 12.5 ppm (Fig. 3c), respectively, which are indicative of the presence of −OH terminations [45]. Similar to the assignment of ^1H signal, the peaks in ^{19}F spectra can be assigned to −F functional group [45]. Besides, they also employed ^1H–^{19}F heteronuclear correlation (HETCOR) spectrum to study the spatial arrangement of the different termination groups (Fig. 3e and f), suggesting that mixed functional groups rather than a single type of terminations existed on the surface of MXenes.

3. Energy applications

3.1. Supercapacitors

A requisite step for exploiting the unique properties of MXenes in energy storage and conversion devices is the intercalation and delamination. Mashtalir and co-workers discovered that layered MXene can accommodate various organic molecules between its layers [27]. It was found that surface functionalized Ti_3C_2 can be intercalated by hydrazine, *N*,*N*-dimethylformamide (DMF) and urea, while hydrazine was directly intercalated into Ti_3CNT_x and $TiNbCT_x$. The delamination of $Ti_3C_2T_x$ sheets was obtained by the intercalation of DMSO into the sheets, followed by the sonication in water, from which MXene paper was prepared, exhibiting a better Li-ion capacity than its non-delaminated counterpart [27]. Recently, the same group further unveiled the spontaneous intercalation of a variety of cations such as Li^+, Na^+, K^+, Mg^{2+}, Al^{3+} and NH_4^+ into MXene layers [28]. Once Li^+ was intercalated into the $Ti_3C_2T_x$ sheets, ion-exchange reactions with various cations can occur, which enables the insertion of other alkali and alkaline earth cations, even larger polyatomic cations into MXenes [53,54]. For instance, Ghidiu et al. discovered that trimethylalkylammonium (AA) cations with increasing alkyl chain length had the capability of ion-exchanging with Li^+, leading to an expansion of interlayer space with little enhancement in the capacitance [53].

The wetting process of MXenes in ionic liquids evidenced a drastic and irreversible volume expansion, which indicated spontaneous ion intercalation, while reversible expansion and contraction of MXenes was also discovered during the voltage cycling [55]. The observed large volumetric changes may require

MXenes layers pillaring with polymers or small molecules prior to the use as supercapacitor electrodes.

$Ti_3C_2T_x$ is the most well studied MXene in supercapacitors. In an early attempt, flexible $Ti_3C_2T_x$ paper was prepared as the electrodes with a volumetric capacitance of 350 F cm^{-3} in NaOH solution [28]. Later, Ghidiu et al. fabricated $Ti_3C_2T_x$ 'clay', which can be rolled, molded and painted to form free-standing flexible films and conductive coatings with desired shapes (Fig. 4a) [23]. As shown in Fig. 4b and c, the rolled films showed the shearing of MXene sheets and poor alignment of flakes, in particular with thicker films. The formed supercapacitor electrodes showed a high volumetric capacitance of 900 F cm^{-3} and almost 100% retention even after 10,000 cycles (see Fig. 4f and g). In a more recent report, Li et al. improved the gravimetric capacitance of $Ti_3C_2T_x$ from 245 F g^{-1} to 517 F g^{-1} via cation intercalation and removal of termination groups such as −OH/−F, which resulted from the increased interlayer voids and more active sites participating in redox reactions [56].

The mechanism of high capacitance in $Ti_3C_2T_x$ was probed by Lukatskaya and co-workers using in-situ X-ray absorption spectroscopy [57]. It was uncovered that $Ti_3C_2T_x$ predominantly served as pseudocapacitive electrode in H_2SO_4 electrolyte, which resulted from the unique properties of $Ti_3C_2T_x$—the spontaneous intercalation of ions into $Ti_3C_2T_x$ layers offers a path for electrochemically active Ti-layer, while the C-layer ensures fast charge transfer. The pseudocapacitance of $Ti_3C_2T_x$ in H_2SO_4 electrolyte was also attributed to the changes of valance state of Ti during the reversible bonding/de-bonding processes between surface terminations and electrolyte [58]. Specifically, the terminal O on the surface of $Ti_3C_2T_x$ was bonded with hydronium in H_2SO_4 upon discharging, while de-bonded upon charging, thus giving rise to the continuous changes of titanium oxidation state during cycling. Besides, charge storage featured by ion exchange accounted for more accommodation of the extremely mobile hydronium into the deep adsorption sites in the $Ti_3C_2T_x$ interlayers, which yielded superior performance of the MXene electrodes in H_2SO_4 electrolyte [58].

Not only inorganic materials including reduced graphene oxide (RGO) [59,60], carbon nanotube (CNT) [59] and onion-like carbon (OLC) [59] but also polymers such as polypyrrole (PPy) [61], polydiallyldimethylammonium chloride (PDDA) [62], and polyvinyl alcohol (PVA) [63] can constitute the composites with $Ti_3C_2T_x$ to increase electronic conductivity, enlarge interlayer spacing and enhance mechanical stability, all of which further improve the

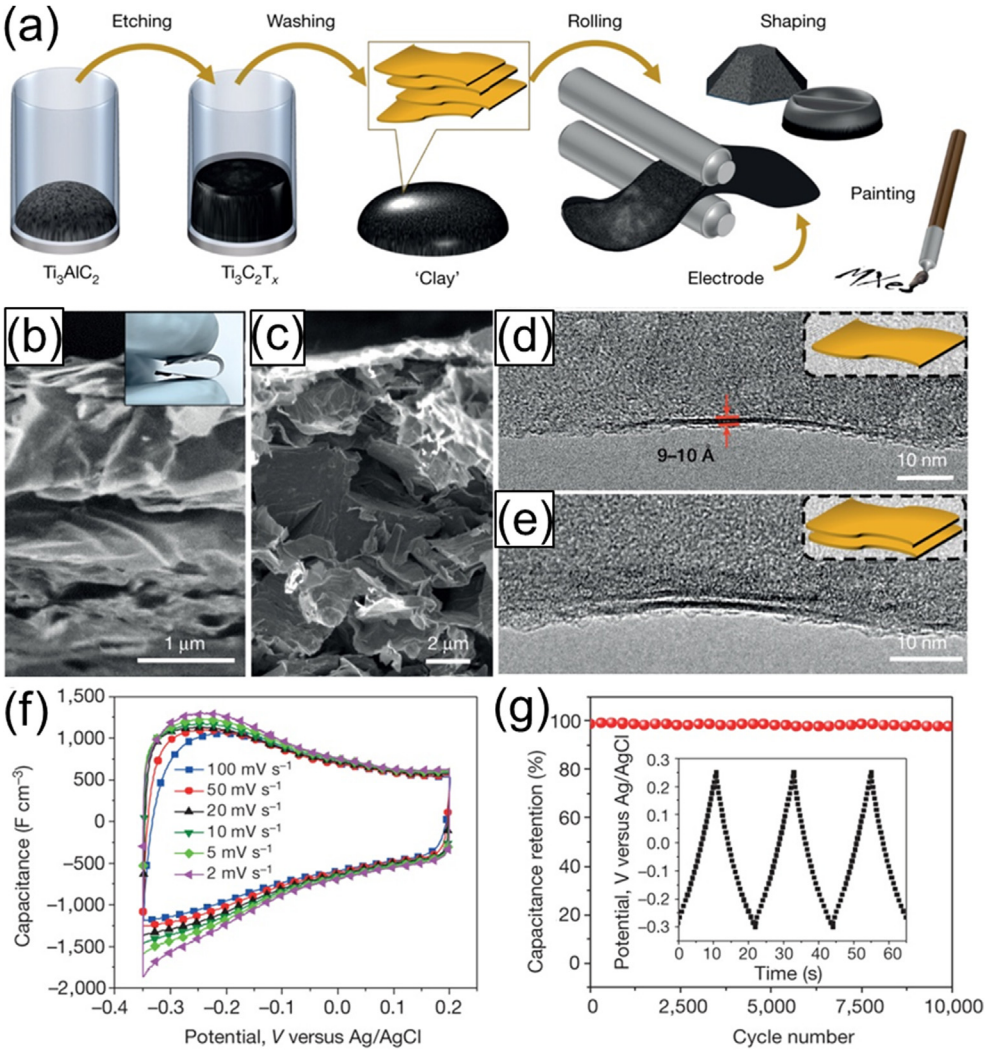

Fig. 4. $Ti_3C_2T_x$ MXene clay and electrode obtained via etching and rolling. (a) Schematic illustration of the fabrication process. (b) SEM image of a 4 μm-thick film. (c) SEM image of a 30 μm-thick film. TEM images of (d) single and (e) double $Ti_3C_2T_x$ layer flakes. Insets are sketches of the layers. (f) Cyclic voltammetry profiles of a 5 μm-thick film at different scan rates in 1 M H_2SO_4. (g) Capacitance retention of 5 μm-thick film in 1 M H_2SO_4. Reproduced with permission from Ref. [23]. Copyright 2014, Nature Publishing Group.

performance of MXene-based electrodes in electrochemical capacitor applications.

In a recent work, Zhao et al. obtained free-standing, flexible and sandwich-like $Ti_3C_2T_x$/CNT paper using a method of alternating filtration [59]. Compared to pure $Ti_3C_2T_x$ and a random mixture of $Ti_3C_2T_x$ and CNT, the electrode materials based on $Ti_3C_2T_x$/CNT paper showed a volumetric capacitance of 350 F cm^{-3} at 5 A g^{-1} without degradation even after 10000 cycles, while the sandwich-like $Ti_3C_2T_x$/single-walled CNT paper displayed a high volumetric capacitance of 390 F cm^{-3} at 2 mV s^{-1} [59]. Moreover, the fabrication protocol can be applied to form sandwich-like MXene/OLC and MXene/RGO paper, while the sandwich-like $Ti_3C_2T_x$/RGO achieved a higher volumetric capacitance of 435 F cm^{-3} with an outstanding cycling stability [59]. In a subsequent report by the same team, $Ti_3C_2T_x$/RGO composites with various amount of RGO were synthesized [60]. The $Ti_3C_2T_x$/RGO electrodes with a weight ratio of 7:1 exhibited a high capacitance of 154.3 F g^{-1} at 2 A g^{-1} and excellent capacity retention of 124.7 F g^{-1} at 4 A g^{-1} after 6000 cycles. In this respect, the RGO served as not only a conductive bridge connecting $Ti_3C_2T_x$ blocks, but also a matrix to reduce the volume change, which greatly enhance the cycling stability during charge/discharge process [60].

In 2014, MXenes/polymer composite was first studied by Ling and co-workers [62]. The researchers mixed $Ti_3C_2T_x$ with a charged PDDA and an electroneutral PVA, respectively, to prepare multifunctional nanocomposites. In comparison to neat PVA or $Ti_3C_2T_x$ films, the flexible $Ti_3C_2T_x$/PVA composite film showed an increase of mechanical strength, a high conductivity of 2.2×10^4 S m^{-1} and an outstanding volumetric capacitance as high as 528 F cm^{-3} at 2 mV s^{-1} [62]. Recently, the Gogotsi group employed an in-situ oxidant-free polymerization method to synthesize PPy/$Ti_3C_2T_x$ composites with excellent electrochemical performance (Fig. 5a) [61]. As shown in Fig. 5b and c and, these films were composed of well-aligned and stacked $Ti_3C_2T_x$ sheets with an alternating arrangement of PPy and MXene. A remarkably high volumetric capacitance of ~1000 F cm^{-3} with 92% capacitance retention after 25,000 charge/discharge cycles was achieved, which rendered them excellent electrode materials for supercapacitors. Such superior performance resulted from not only the self-assembled layered structure but also the synergistic effect of surface redox processes and extended interlayer space of $Ti_3C_2T_x$. Inspired by that, Zhu and co-workers developed a flexible and conductive film via intercalating PPy into the Ti_3C_2 layers during the electrochemical polymerization process, which improved the capacitance from 300 to 406 F cm^{-3} and attained almost 100% capacitance retention after 20,000 cycles [63]. In their work, the layered Ti_3C_2 effectively prevented PPy from dense stacking and hence high electrochemical activity of PPy was maintained. Moreover, owing to the strong bonds formed between the Ti_3C_2 surface and PPy chains, facile pathways for both charge transport and structural stability were created [63]. In a more recent report, Luo et al. fabricated cetyltrimethylammonium bromide (CTAB)–Sn(IV)@Ti_3C_2 by the method of CTAB and Sn^{4+} pillaring, which reached a large interlayer spacing of ~2.7 nm with an excellent energy density [64].

Micro-supercapacitors (MSC) are of vital importance to microscale and wearable electronic devices. Considerable attempts have been made in conventional microfabrication techniques, yet the research on MXenes-based MSCs is still lacking. Kurra and co-workers presented the fabrication of MXene-on-paper coplanar MSCs via the Meyer rod coating method followed by laser machining, which could be applied to produce other coplanar and flexible energy storage devices [65]. They proposed that both the etching process and the morphology of $Ti_3C_2T_x$ played important roles in the electrochemical performance of MSCs due to their physical dimensions, interlayer space and conductivity. An all-MXene solid-state MSC was later fabricated by Peng and co-workers via a sequence of solution spray-coating and direct laser cutting methods, which consisted of large-flake $Ti_3C_2T_x$ serving as current collectors and small-flake $Ti_3C_2T_x$ with defects and edges as the active layer (Fig. 6) [66]. The corresponding MSC devices exhibited the areal and volumetric capacitances of 27.3 mF cm^{-2} and 356.8 F cm^{-3} at 0.2 mA cm^{-2}, respectively, with excellent capacitance retention of 100% after 10,000 cycles at 50 mV s^{-1}.

Recent years have also seen increased research activities on other potential MXenes with excellent electronic properties and intercalation behavior including Ti_2CT_x, Nb_2CT_x, Mo_2CT_x. For instance, Rakhi et al. recently found that ambient atmosphere of post-annealing greatly influenced the structural and electrochemical properties of MXene [67]. Ti_2CT_x annealed in N_2/H_2 mixed atmosphere delivered a maximum capacitance of 51 F g^{-1} at 1 A g^{-1} and a high rate performance of 86% with 93% capacitance retention after 6000 cycles. The excellent performance is due to not only the lowest fluorine content and the highest carbon content on the surface of Ti_2CT_x, but also the thorough expose of electrodes to aqueous electrolyte ensured by retaining layered MXene [67]. Chloride termination groups were observed in Ti_2CT_x, which significantly expanded the interlayer space and further increased the Li^+ accessibility. As-produced Ti_2CT_x electrodes yielded unprecedentedly large capacitance of 300 F g^{-1} [68]. In a more recent report, Halim et al. synthesized Mo_2CT_x by selectively etching gallium from Mo_2Ga_2C, which exhibited semiconductor-like behavior distinct than of $Ti_3C_2T_x$ [69]. The 2 μm-thick supercapacitor electrodes based on Mo_2CT_x showed a high capacitance of 700 F cm^{-3} in 1 M H_2SO_4 with excellent capacitance retention of almost 100% after 10000 cycles. In a very recent study, Zhang et al. acquired orthorhombic niobium pentoxide (T-Nb_2O_5)/carbon/Nb_2CT_x composite via a one-step CO_2 oxidation of Nb_2CT_x [70]. As-fabricated hierarchical 50 μm-thick electrodes achieved a high capacitance of 660 mF cm^{-2} over a charge/discharge time of 4 min because of the pseudocapacitive response and fast rate of T-Nb_2O_5 as well as the high conductivity of the residual Nb_2CT_x and disordered carbon.

Table 1 summarizes the performance of MXene-based electrodes for supercapacitors as above reviewed. For the sake of comparison, several conventional electrodes used in supercapacitors are also provided. Compared to typical electrode materials such as graphene and MoS_2, a combination of intriguing characteristics in MXenes such as good electrical conductivity, mechanical stability, high specific surface area and flexibility leads to relatively higher capacitance even at high scan rates and better cycling performance. Among various MXenes and their composites, flexible and free-standing PPy/$Ti_3C_2T_x$ fabricated by in-situ polymerization exhibited the highest volumetric capacitance with unprecedented charge/discharge stability, which holds great promise for new-generation electrochemical capacitors. Moreover, a variety of composites containing small molecules or polymers have significantly improved the performance of their parent MXenes. MXenes are also particularly suitable for MSC applications and binder-free devices due to their large capacitance delivered even for several-micrometer-thick film electrodes. Despite the mostly studied $Ti_3C_2T_x$ as stated above, other MXenes with different compositions remain to be further explored, including materials design, fabrication methods and devices configurations.

3.2. Batteries

The working mechanism of batteries is the shuttle of ions between electrodes through a liquid ion electrolyte [73]. Ions are extracted from anode and then inserted into the cathode during discharge process. During charging, the opposite process occurs. The electrodes thus play a substantial role on the battery

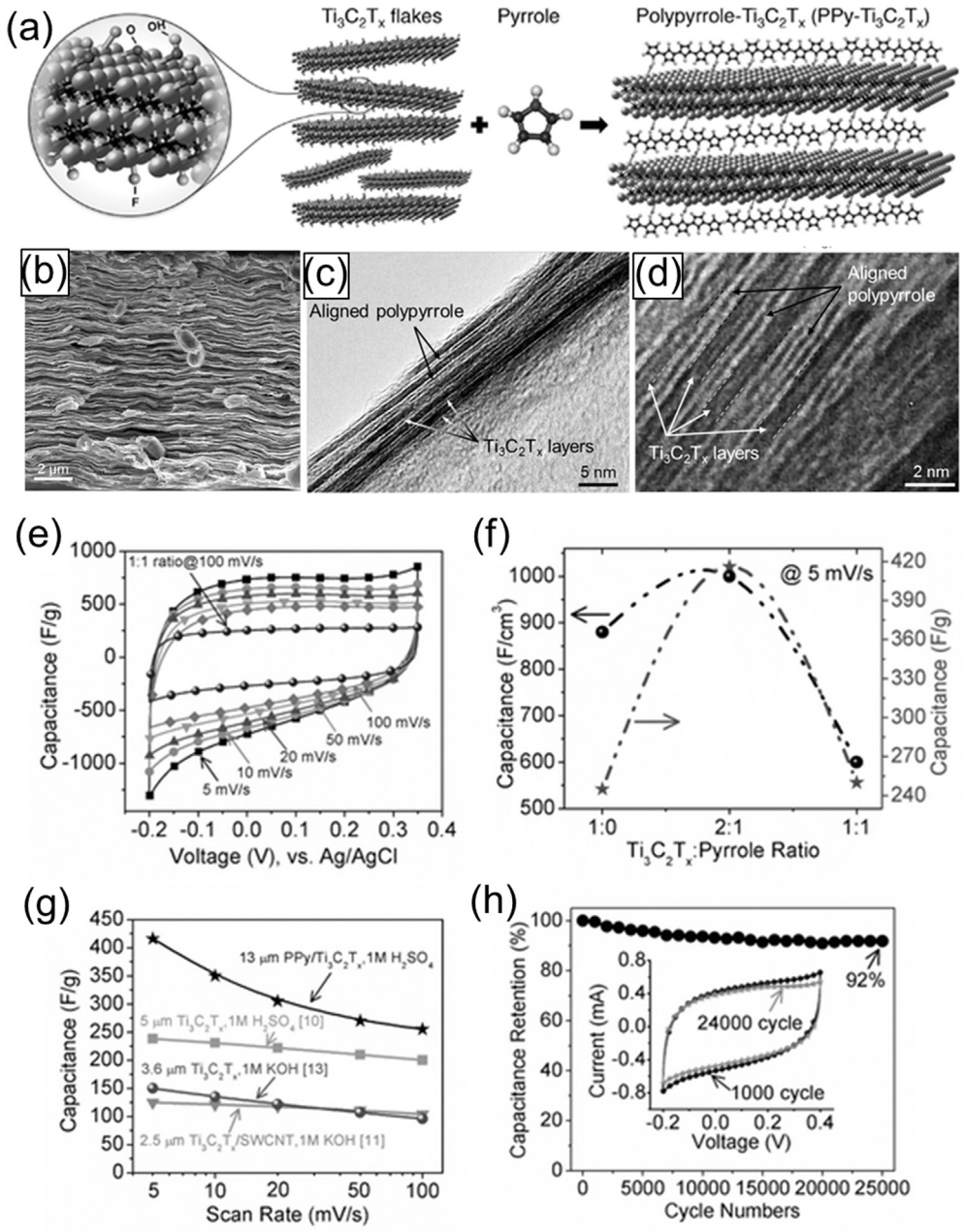

Fig. 5. PPy/$Ti_3C_2T_x$ composite produced by in-situ oxidant-free polymerization method. (a) Schematic illustration of in-situ polymerization using MXene. (b) SEM image of PPy/$Ti_3C_2T_x$ film. (c,d) TEM images of aligned PPy chains between $Ti_3C_2T_x$ sheets. (e) Cyclic voltammetry profiles of PPy/$Ti_3C_2T_x$ (1:2) film at different scan rates. (f) Effect of PPy and $Ti_3C_2T_x$ ratio on volumetric (left-side y-axis) and gravimetric (right-side y-axis) capacitance at 5 mV s^{-1}. (g) Comparisons of PPy/$Ti_3C_2T_x$ (1:2) film with other $Ti_3C_2T_x$ electrodes. (h) Cycle life performance of PPy/$Ti_3C_2T_x$ (1:2) film. Reproduced with permission from Ref. [61]. Copyright 2015, John Wiley & Sons.

performance. To obtain high-performance batteries, ideal electrode materials should combine high surface-to-volume ration, outstanding electrochemical properties and good mechanical stability. Graphite is the most widely used electrode materials for Li-ion batteries (LIBs) owing to its high columbic efficiency and flat potential profile; however, its low theoretical capacity hampers the further development [32]. Numerous efforts have thus been made to explore alternative electrode materials with better performance. In early attempts, conventional 2D materials such as graphene [74] and graphene-based composites [75,76] have been employed as electrodes, due to their large surface areas and efficient ion transport between their layers. Recently, MXenes has also been used as promising electrodes, since they can spontaneously adsorb proper cations with potential redox reactions on active sites, thereby permitting relatively large capacity of corresponding batteries. It was theoretically predicted that Ti_3C_2 was capable of adsorbing alkali metal ions such as Li^+, Na^+, Ca^{2+} and K^+, giving theoretical capacities of 447.8, 351.8, 319.8 and 191.8 mAh g^{-1}, respectively [77].

MXenes can not only store large amounts of electrical charges, but also discharge at rapid rates, which is in sharp controversy to other conventional anodes materials. Therefore, Levi et al. investigated this paradox of the capacity of 2D MXenes by using complementary methods of in-situ electronic conductance measurements and electrochemical quartz-crystal admittance [78]. It was revealed that cationic insertion and deformation of MXenes

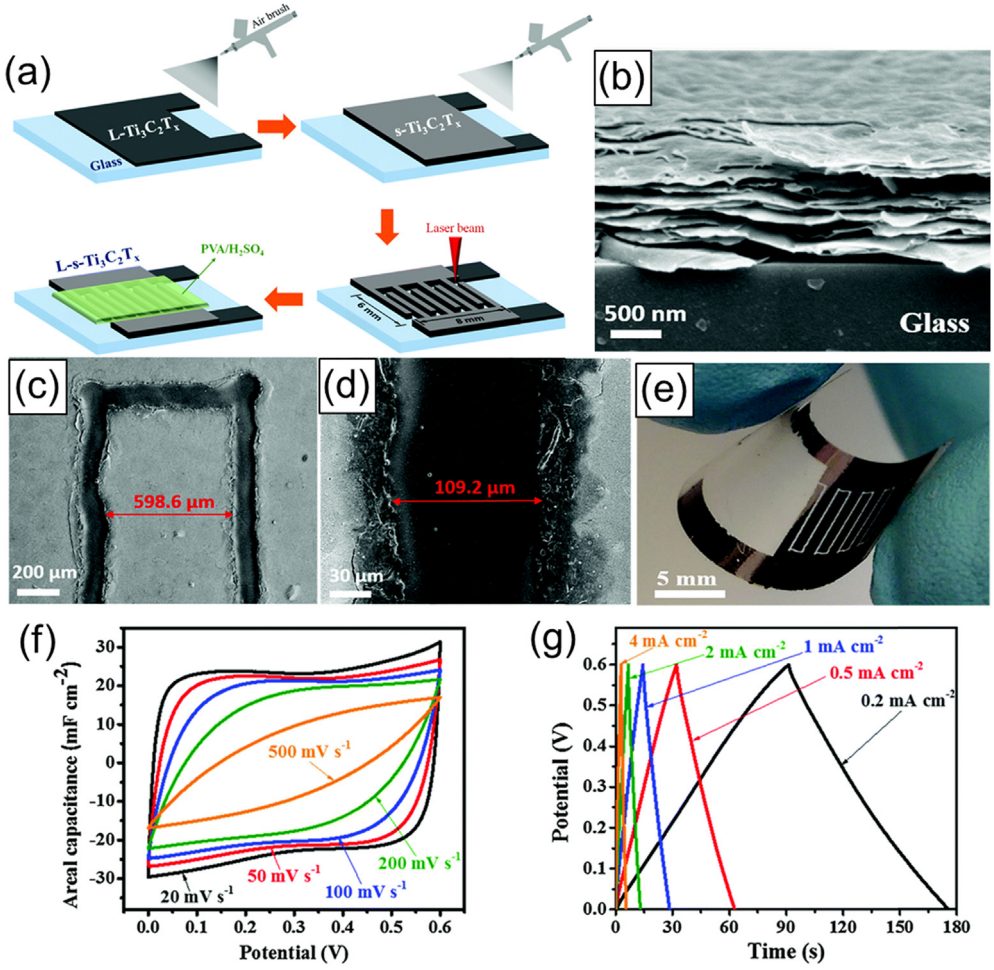

Fig. 6. All-$Ti_3C_2T_x$ MXene MSCs produced via spray-coating and laser cutting. (a) Schematic illustration of the fabrication process. (b) Cross-sectional SEM image of $Ti_3C_2T_x$. SEM images of (c) $Ti_3C_2T_x$ electrode and (d) the interspace region. (e) Digital photograph showing transferred MSC on flexible scotch tape. (f) CV curves of $Ti_3C_2T_x$ MSCs at different scan rates. (g) Cycle profiles of $Ti_3C_2T_x$ MSCs at different current densities. Reproduced with permission from Ref. [66]. Copyright 2016, the Royal Society of Chemistry.

can be facilitated by the existence of H_2O between MXene nanosheets, which contributed to the capacitive paradox of MXene electrode materials. Sun et al. interpreted such capacitive features in LIBs based on MXene electrodes by structural transformation and electrochemical reactions [79]. They classified O-terminated MXenes (M_2CO_2) into two types, V-type (M = V, Cr and Ta) and Sc-type (M = Sc, Ti, Zr, Nb and Hf), depending on whether the structural transformation exists or not during the process of adsorbing the first Li layer [79]. The details are shown in Fig. 7. Specifically, V-type M_2CO_2 with reversible structural transformation preferred the sandwich configuration (i.e., H_2H_1T-$M_2CO_2Li_4$) while the TH_1H_2-$M_2CO_2Li_4$ structure is favorable for the Sc-type M_2CO_2 except for Nb_2CO_2 during the adsorption of further Li. For example, the H_2H_1T-$V_2CO_2Li_4$ delivered a large capacity of 735 mAh g^{-1}, accounting for such structural transformation that prevented the formation of Li dendrite from additional Li atoms [79].

Another important performance parameter of batteries is cycle life, which is greatly affected by the mechanical strain and stress resulting from volumetric change during electrochemical reactions. Come et al. investigated the elastic changes of $Ti_3C_2T_x$ pseudocapacitive electrodes, suggesting that the cations content was strongly correlated with the out-of-plane elastic modulus [80]. It is worth noting that the presence of water led to the more than doubled stiffness of $Ti_3C_2T_x$ in the direction perpendicular to the basal plane on Li^+ intercalation. Moreover, a combination of in-situ imaging and DFT calculation provides a viable avenue to track and distinguish the superior intercalation paths on the nanoscale, which is of critical importance to understand the ionic transport in MXenes.

Continuous efforts have been devoted to fabricate high-performance LIBs. Several emerging strategies, such as tuning the composition, doping and hybridization [30], were utilized to further improve the performance of MXenes anodes. With regard to most studied titanium carbides (Ti_3C_2), Luo et al. fabricated polyvinylpyrrolidone (PVP)-Sn(IV)@Ti_3C_2 nanocomposites by facile PVP-assisted liquid-phase immersion process [81]. As-synthesized nanocomposites possessed excellent reversible capacity of 635 mAh g^{-1} at 100 mA g^{-1} and exhibited outstanding cycling stability after 50 cycles due to the synergistic effects of the Sn and alkalization-intercalated Ti_3C_2 matrix along with potential “pillar effect” of Sn between alk-Ti_3C_2 layers. Recently, a new MXene/Ag composite was synthesized and used as anode material for LIBs via directly reducing $AgNO_3$ aqueous solution in contact with $Ti_3C_2(OH)_{0.8}F_{1.2}$, revealing an extraordinary long cycle lifetime of >5000 cycles without capacity decay at 1–50 C with a rapid charge-discharge rate (Fig. 8), which could be attributed to the reduced interface resistance and the existence of Ti(II) to Ti(III) in the cycling process [82]. Tesfaye and co-workers reported the anodization of Ti_3SiC_2 in a HF-containing electrolyte to prepare the negative electrode for LIBs [83]. The anodized Ti_3SiC_2 were mostly

Table 1
Performance summaries of MXenes and their composites in comparison to conventional materials when used as supercapacitor electrodes.

Material	Electrolyte	Performance	Configuration	Ref.
Metallic 1 T MoS_2	0.5 M H_2SO_4, Li_2SO_4, Na_2SO_4, K_2SO_4 KCl or KBr	400–700 F cm^{-3}, ~90% retention after 5000 cycles	Three-electrode Swagelok cells	[71]
Graphene (cathode)/porous graphene (anode) $Ni(OH)_2$	6 M KOH	218.4 F g^{-1}, ~94% retention after 3000 cycles at 100 mV s^{-1}	Two-electrode device	[72]
$Ti_3C_2T_x$	1 M H_2SO_4	900 F cm^{-3}, almost 100% retention after 10000 cycles	Three-electrode Swagelok cells	[23]
$Ti_3C_2T_x$	KOH	340 F cm^{-3}, almost 100% retention after 10000 cycles	Three-electrode Swagelok cells	[28]
$Ti_3C_2T_x$	1 M H_2SO_4 and PVA/H_2SO_4 gel	25 mF cm^{-2} at 20 mV s^{-1}, 92% retention after 10000 cycles	Two-electrode device	[65]
$Ti_3C_2T_x$	1 M H_2SO_4, Li_2SO_4, Na_2SO_4, and K_2SO_4	517 F g^{-1} at 1 A g^{-1}, 99% retention after 10000 cycles	Three-electrode Swagelok cells	[56]
$Ti_3C_2T_x$ (MSC)	PVA/H_2SO_4 gel	27.3 mF cm^{-2} and 356.8 F cm^{-3} at 0.2 mA cm^{-2}, 100% retention after 10000 cycles	Two-electrode devices	[66]
Mixed $Ti_3C_2T_x$/SWCNT	1 M $MgSO_4$	300 F cm^{-3} at 2 mV s^{-1}	Three-electrode Swagelok cells	[59]
Sandwich-like $Ti_3C_2T_x$/SWCNT	1 M $MgSO_4$	390 F cm^{-3} at 2 mV s^{-1}, no degradation after 10000 cycles	Three-electrode Swagelok cells	[59]
Mixed $Ti_3C_2T_x$/MWCNT	1 M $MgSO_4$	366 F cm^{-3} at 2 mV s^{-1}	Three-electrode Swagelok cells	[59]
Sandwich-like $Ti_3C_2T_x$/RGO	1 M $MgSO_4$	435 F cm^{-3} at 2 mV s^{-1}, increase from 340 to 370 F cm^{-3} at 10 A g^{-1} over 10000 cycles	Three-electrode Swagelok cells	[59]
Sandwich-like $Ti_3C_2T_x$/OLC	1 M $MgSO_4$	397 F cm^{-3} at 2 mV s^{-1}	Three-electrode Swagelok cells	[59]
$Ti_3C_2T_x$/RGO (weight ratio: 7:1)	2 M KOH	154.3 F g^{-1} at 2 A g^{-1}, 124.7 F g^{-1} at 4 A g^{-1} after 6000 cycles	Three-electrode cells	[60]
$Ti_3C_2T_x$/PVA	1 M KOH	528 F cm^{-3} at 2 mV s^{-1}, 314 F cm^{-3} after 10000 cycles	Three-electrode Swagelok cells	[62]
PPy/$Ti_3C_2T_x$ (in situ polymerization)	1 M H_2SO_4	1000 F cm^{-3}, 92% capacitance retention after 25000 cycles	Three-electrode Swagelok cells	[61]
PPy/$Ti_3C_2T_x$ (electrochemical polymerization)	Solid-state PVA-H_2SO_4	406 F cm^{-3}, almost 100% capacitance retention after 20000 cycles		[63]
CTAB–Sn(IV)@$Ti_3C_2T_x$	1 M $LiPF_6$ in ethylene carbonate (EC)/dimethyl carbonate (DEC)/ethyl methyl carbonate (EMC)	181 F g^{-1} at 1 A g^{-1}, ~71% capacitance retention after 4000 cycles at 2 A g^{-1}	CR2032-type coin cells	[64]
Ti_2CT_x (anneal in N_2/H_2)	30 wt % KOH aqueous	51 F g^{-1} at 1 A g^{-1}, 93% capacitance retention after 6000 cycles	Two-electrode, symmetric devices	[67]
Ti_2CT_x	1 M $LiPF_6$ in EC/dimethyl carbonate (DMC)	130 F cm^{-3}, 300 F g^{-1}	CR2032-type coin cells	[68]
Mo_2CT_x	1 M H_2SO_4	700 F cm^{-3}, almost 100% retention after 10000 cycles	Three-electrode Swagelok cells	[69]
(T-Nb_2O_5)/carbon/Nb_2CT_x	1 M $LiClO_4$ in EC/DMC	660 mF cm^{-2}	Three-electrode Swagelok cells	[70]

comprised of anatase and a small quantity of SiO_2 and carbon. A capacity of 380 μAh cm^{-2} was acquired after 140 cycles, which were higher than that of amorphous titania, resulting from the remaining nonanodized MAX phase and/or the existence of sp^2-bonds of disordered carbons.

Moreover, other 2D TMCs and TMNs such as Nb_2CT_x, $Nb_4C_3T_x$, Mo_2C, V_2CO_2 and $V_4C_3O_2$ have been theoretically and experimentally investigated. For instance, Mashtalir and co-workers produced Nb_2CT_x/CNT paper electrodes with a capacity of >400 mAh g^{-1} at 0.5 C and a volumetric capacitance of 325 F cm^{-3} in LIBs [44]. Orthorhombic Nb_2O_5@$Nb_4C_3T_x$ or Nb_2CT_x hierarchical composites were fabricated by one-step oxidation, that is, flowing CO_2 oxidized $Nb_4C_3T_x$ (or Nb_2CT_x) at 850 °C for 30 min [84]. The as-received Nb_2O_5@$Nb_4C_3T_x$ composites showed reversible capacities of 208 mAh g^{-1} at a rate of 50 mA g^{-1} at 0.25 C in 1–3 V versus Li^+/Li, and retained 94% capacity with 100% Coulombic efficiency after 400 cycles. Sun et al. employed first-principles calculations to identify a stable anode material, Mo_2C monolayer, showing minor diffusion barriers of 0.035 eV for Li-ion batteries, which suggested its excellent diffusion mobility and cycling ability [85]. Besides, the Li-absorbed Mo_2C monolayer exhibited a calculated electrochemical capacity of 526 mAh g^{-1} [85]. Ashton et al. computationally studied MXene anodes in LIBs and predicted that V_2CO_2 had the largest reversible capacity with the highest diffusion barrier while $V_4C_3O_2$ yielded the lowest reversible capacity with the fastest diffusion rate [86].

Lithium-sulfur batteries (LSBs) have recently become a significant research area because the sulfur (S) element is abundant, cost-effective and environmentally friendly. However, the absence of appropriate host materials for sulfur and lithiated derivatives is an obstacle for the development of high-performance LSBs [31,87]. Thus, Liang and co-workers created 70 wt% S/Ti_2C composites as hosts in LSBs via the reaction between S and the hydrophilic surface of Ti_2C [88]. Therefore, the polysulfide species strongly interacted with Ti atoms on the surface. As a result, the positive electrode showed a capacity of ~1200 mAh g^{-1} at 0.2 C and retained 80% capacity after 400 cycles at 0.5 C.

Another type of hybrid batteries, Mg/Li-ion batteries (MLIBs), can be also made based on MXenes. For example, Byeon and co-workers reported the use of $Ti_3C_2T_x$ and Mo_2CT_x as the cathode materials, in which flexible $Ti_3C_2T_x$/CNT paper electrode achieved a capacity of 100 mAh g^{-1} at 0.1 C and remarkable capacity retention of 80 mAh g^{-1} at 1 C after over 500 cycles, while the Mo_2CT_x cathode showed higher capacities only [89].

In addition to the active research on MXene-based Li^+-containing batteries, the search of MXenes for non-Li^+ batteries have been recently made. For instance, Xie et al. theoretically predicted that not only Na^+ and K^+ but also other multivalent metal ions such

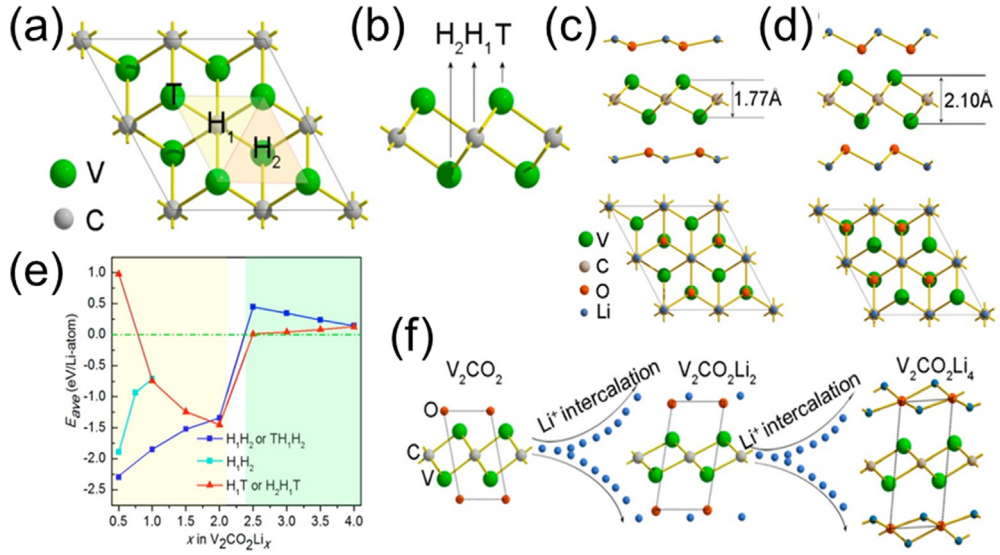

Fig. 7. Schematic showing the structures of V_2C with (a) top and (b) side views. Side and top views of (c) H_1T-$V_2CO_2Li_2$ and (d) H_1H_2-$V_2CO_2Li_2$. (e) The dependences of E_{av} on Li contents (x) in V_2CO_2. The light and dark blue lines H_1H_2 represent that the Li atoms in first layer are located at H_1 sites on both sides and one side of H_2-V_2CO_2, respectively. The red line H_1T represents that the Li atoms are located at H_1 sites on both sides of T- V_2CO_2. TH_1H_2 and H_2H_1T represent that the Li atoms in the second layer are located at T sides on H_2-V_2CO_2 and H_2 sides on T-V_2CO_2, respectively. (f) Schematic illustration of the structure transformation during the adsorption of the first Li layer. Reproduced with permission from Ref. [79]. Copyright 2015, American Chemical Society. (For interpretation of the references to colour in this figure legend, the reader is referred to the web version of this article.)

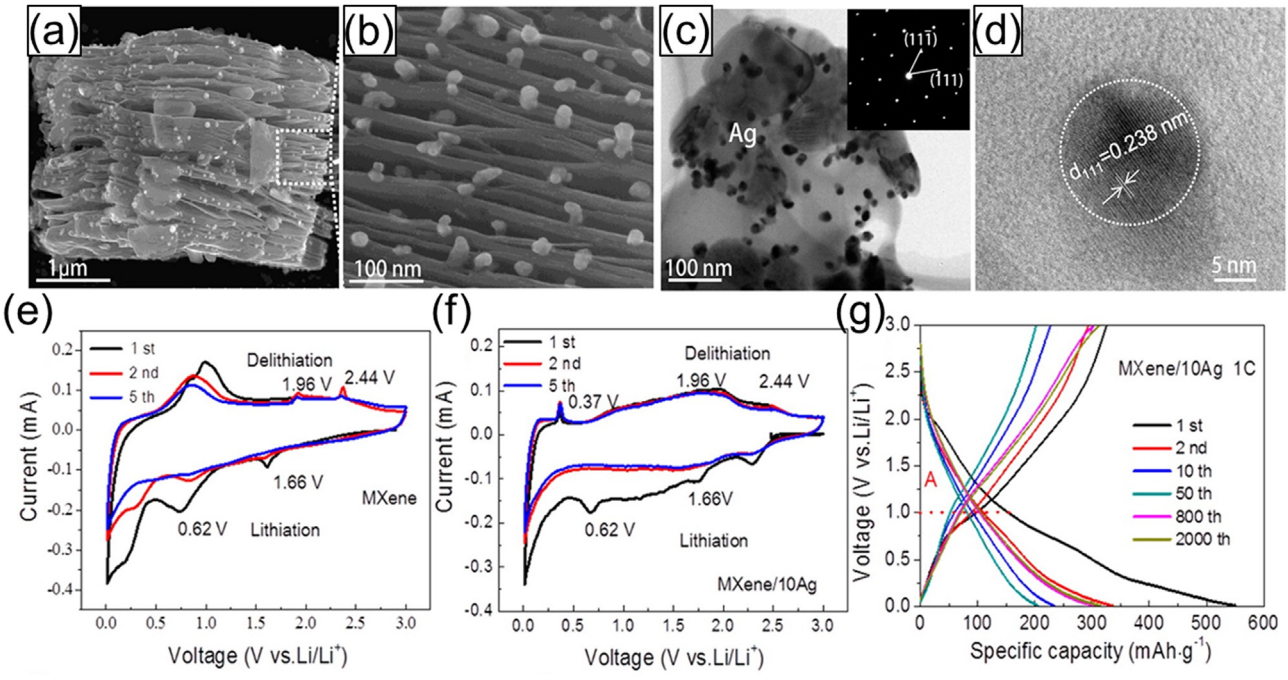

Fig. 8. MXene/10Ag composites: (a) SEM image and (b) its high-magnification graph. (c) TEM image and (d) its high-resolution graph of a Ag particle. CV curves of (e) neat MXene and (f) composites. (g) Charge/discharge curves at 1 C. Reproduced with permission from Ref. [82]. Copyright 2016, American Chemical Society.

as Mg^{2+} and Al^{3+} can be stored in MXene based multilayers via combined mechanisms of conversion reaction, insertion/extraction and plating/stripping, if kinetically allowed [90]. It was then experimentally demonstrated that Na^+ and K^+ were successfully intercalated into MXene nanosheets, in which bare MXenes theoretically showed better rate capabilities and higher capacities than the O-terminated ones. Eames et al. further studied the intercalation of those metal ions, indicating that both the transition metal species and surface functional groups played dominant roles in the voltage and capacity of MXene-based batteries [91].

On the other hand, Yu applied ab initio density functional theory to investigate systemically the sodiation process on the surfaces of interlayer-expanded bare and chemically functionalized Ti_3C_2 [92]. The results suggested that Na-ion batteries (NIBs) based on MXene intercalation hosts had lower sodium diffusion barriers, improved sodium storage capacities and small volume change. In this regard,

both the bare and O-functionalized Ti_3C_2 with enlarged interlayer distance can serve as promising anode materials because their diffusion barriers are 0.02, and 0.20 eV, respectively, and the storage capacities are greater than 413.0 and 367.7 mAh g^{-1}, respectively. Kajiyama et al. further studied the sodium-ion intercalation mechanism in $Ti_3C_2T_x$ by ^{23}Na magic angle spinning NMR (^{23}Na MAS NMR) spectroscopy and DFT method, showing the reversible intercalation/deintercalation of Na^+ into $Ti_3C_2T_x$ in a nonaqueous electrolyte, due to the extension of the interlayer distance in the first sodiation process (Fig. 9a and b) [93]. Furthermore, the nearly unchanged interlayer distance during sodiation/de-sodiation was ascribed to both the swelling effect of impregnated solvent molecules between interlayer space and the pillar effect of trapped Na^+ (Fig. 9c and d). Thus no substance was changed during the electrochemical reaction and good capacity retention after 100 cycles was achieved. Recently, Wang et al. fabricated Na-ion full cell comprising a Ti_2C negative electrode and an alluaudite $Na_2Fe_2(SO_4)_3$ positive electrode, showing capacities of 90 mAh g^{-1} at 1.0 A g^{-1} and 40 mAh g^{-1} at 5.0 A g^{-1} at 2.4 V on the basis of the Ti_2C weight [94]. Without significant structural changes, the pseudocapacitance stored more charges at a relatively faster charge/discharge rate than that of the double-layer and ion intercalation.

Except for titanium carbides, V_2CT_x/HC NIBs with a capacity of 50 mAh g^{-1} and a cell voltage of 3.5 V were obtained by Dall'Agnese and co-workers [95]. The authors also unraveled that Na^+ were continuously intercalated between the V_2CT_x layers during the sodiation/de-sodiation processes. The Na-absorbed Mo_2C monolayer exhibited a calculated electrochemical capacity of 132 mAh g^{-1}, which was relatively lower due to the proposed competition mechanism existing in the exchange interaction of Na atoms that was originated from both the Mo_2C monolayer and the surrounding Na atoms [85].

Table 2 summarizes the performance of the above reviewed MXenes-based batteries. Several conventional electrode materials used in batteries are also offered. 2D TMCs and TMNs were used in both LIBs and non-lithium-ion batteries as electrodes, partially owing to their low metal diffusion barrier on the MXene surface. The MXene/Ag composites delivered both superior rate capability and outstanding long-term cycling stability, which offers a novel strategy of fabricating other MXene-metal composites with good electrochemical properties. Besides, MXenes for NIBs and hybrid batteries have been extensively investigated, which yielded a relatively high capacity although the cycling performance needs to be enhanced. Moreover, compared to the specific capacities as theoretically predicted, the devices experimentally produced remain to be further improved.

3.3. Thermoelectric applications

A high-performance thermoelectric (TE) material must afford good electrical conductivity yet poor thermal conductivity. The TE performance is generally characterized by a dimensionless $ZT = S^2\sigma T/\kappa$ where T is the temperature, S is Seebeck coefficient, σ is the electrical conductivity, and κ is the thermal conductivity.

The MAX phases are generally poor TE materials because of their relatively small Seebeck coefficients and high thermal conductivity in metallic systems [97]. In contrast, several MXenes revealed

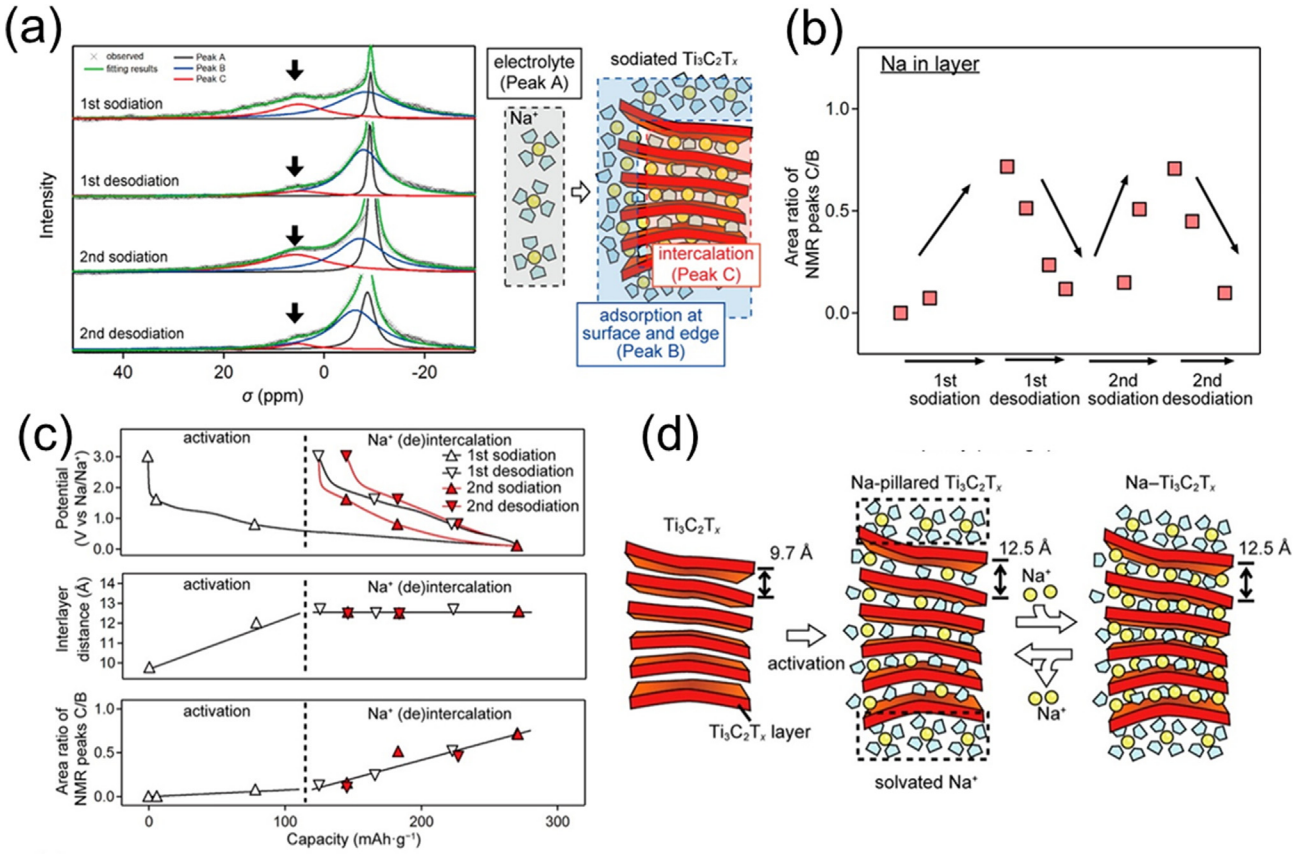

Fig. 9. (a) ^{23}Na MAS NMR signals during the first and the second cycles, where the three peaks originate from different species of Na^+ shown in the schematic illustration. (b) Estimated amount of intercalated Na in MXene layer. (c) Change of the interlayer distance and the intercalated Na amount. (d) Schematic illustration of the mechanism of Na^+ intercalation into $Ti_3C_2T_x$. Reproduced with permission from Ref. [93]. Copyright 2016, American Chemical Society.

Table 2
Performance summaries of MXenes and their composites in comparison to conventional 2D materials when used as battery electrodes.

Material	Type	Electrolyte	Performance	Configuration	Ref.
Graphene	LIB	1 M $LiClO_4$ in EC/DEC	540 mAh g^{-1}	Three-electrode electrochemical cells	[74]
MoS_2/graphene	LIB	1 M $LiPF_6$ in EC/DEC	466 mAh g^{-1} at 4 A g^{-1}, 566 mAh g^{-1} retained after 50 cycles at 0.5 A g^{-1}	Two-electrode coin cells	[75]
Black phosphorus/ graphene	LIB	1 M $LiPF_6$ in EC/DEC/EMC	501 mAh g^{-1} at 0.5 A g^{-1}, ~100% retained after 1000 cycles at 1 A g^{-1}	CR2032-type coin cells	[76]
PVP-Sn(IV) @Ti_3C_2	LIB	1 M $LiPF_6$ in EC/DEC	635 mAh g^{-1} at 100 mA g^{-1}, 50 cycles	Coin-type test cells	[81]
$Ti_3C_2(OH)_{0.8}F_{1.2}$ /Ag	LIB	1 M $LiPF_6$ in EC/DEC/EMC	310 mAh g^{-1} at 1 C, 5000 cycles	Coin-type 2016 cells	[82]
Ti_3SiC_2	LIB	1 M $LiPF_6$ in EC/DEC	380 μAh cm^{-2}, 140 cycles	Two-electrode Swagelok cells	[83]
Nb_2CT_x/CNT	LIB	1 M $LiPF_6$ in EC/DEC	400 mAh g^{-1} at 0.5 C	CR-2016 coin-type cells	[44]
Nb_2O_5@ $Nb_4C_3T_x$	LIB	1 M $LiClO_4$ in EC/DMC	208 mAh g^{-1} at 0.25C, 400 cycles	CR-2016 type half-cells	[84]
70 wt% S/Ti_2C	LSB	1m LiTFSI in DME/1,3-dioxolane (DOL)	1200 mAh g^{-1} at 0.2 C, retain 80% after 400 cycles at 0.5 C	Coin cell	[88]
$Ti_3C_2T_x$/CNT	MLIB	APC + LiCl	80 mAh g^{-1} at 1 C, 500 cycles	Coin-type 2016 cells	[89]
Mo_2CT_x	MLIB	APC + LiCl	120 mAh g^{-1}	Coin-type 2016 cells	[89]
Phosphorene-graphene	NIB	1 M $NaPF_6$ in EC/DEC with 10% fluoroethylene carbonate	1450 mAh g^{-1} at 3 C, 84% retained after 100 cycles at 3 C	CR2032-type coin cells	[96]
$Ti_3C_2T_x$	NIB	1 M $NaPF_6$ in EC/DEC	100 mAh g^{-1}, 100 cycles	CR2032-type coin cells	[93]
Ti_2CT_x	NIB	1 M $NaPF_6$ in EC/DEC	90 mAh g^{-1} at 1 A g^{-1}	CR2032-type coin cells	[94]
V_2C	NIB	1 M $NaPF_6$ in EC/DMC	50 mAh g^{-1}, retain 70% after 300 cycles	Two-electrode Swagelok cells, three-electrode Swagelok cells	[95]

semiconducting properties upon appropriate surface terminations. Regardless of their relatively high thermal conductivity, it was theoretically predicted that semiconducting MXenes had higher Seebeck coefficient and larger electrical conductivity than conventional TE materials, holding good promise of TE applications.

In an initial attempt, Khazaei et al. first-principle calculated that Sc_2CO_2, $Sc_2C(OH)_2$, Sc_2CF_2, Ti_2CO_2, Zr_2CO_2 and Hf_2CO_2 exhibited semiconducting properties [19]. As shown in Fig. 10a and b, for example, the pristine Ti_2C is metallic. When the Ti_2C surface absorbed the F atoms, the Ti_2C remained metallic although each F atom received one electron from MXene and downshifted the Fermi energy level (Fig. 10d). It is apparent from the density of states (DOSs) of Ti_2CO_2 shown in Fig. 10e that each O atom attained two electrons from Ti_2C when O atoms were terminated on the Ti_2C surface, which down-shifted the Fermi energy level to the center of the energy gap. Thus, the Ti_2C became semiconducting after O functionalization. Moreover, their simulations based on the Boltzmann theory revealed that single-layer semiconducting MXene showed very large Seebeck coefficients at low temperatures. For instance, monolayer Ti_2CO_2 and $Sc_2C(OH)_2$ yielded more than 1140 and 2300 μV K^{-1} around 100 K, respectively. The large Seebeck coefficients can be explained by its large contrast of carrier velocities and/or DOS above and below the chemical potential. Furthermore, the same team systematically studied the TE properties of ~35 various functionalized monolayer and multilayer based on MXenes, and proposed that the functionalized Mo_2C presented the most promising TE properties [97]. Mo_2CF_2, in particular, is the most exceptional one. The large Seebeck coefficient and good electrical conductivity of semiconductive MXenes at low carrier concentration make them as potentially excellent TE materials.

However, when the lattice contribution plays a critical role in the above-mentioned electronic quantities, the figures of merits are inefficient to determine the thermoelectric efficiency. Gandi and co-workers thus for the first time predicted the TE properties of MXenes by taking both the phonon and the electron transport into consideration, indicating that the lattice contributed the least to thermal conductivity in Ti_2CO_2 [98]. Their simulation also showed that n-doping in these MXenes resulted in larger Seebeck coefficients owing to the heavier effective mass of electrons.

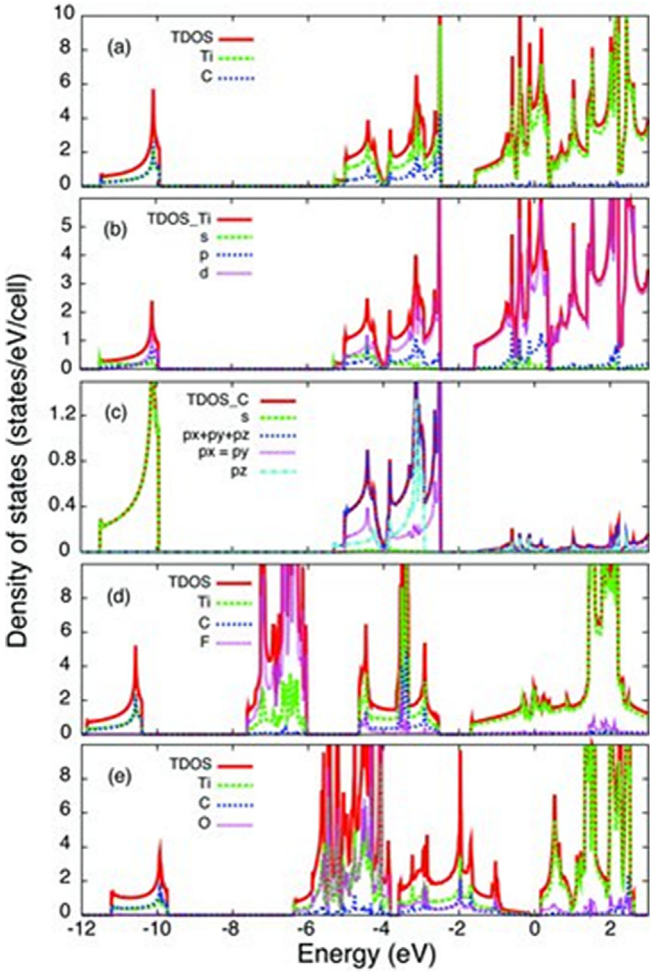

Fig. 10. (a) DOS of Ti_2C, (b,c) Projected densities of states (PDOS) on atomic orbitals of Ti and C atoms, respectively. (d,e) DOS of Ti_2CF_2, and Ti_2CO_2, respectively. Fermi energy is at zero. For the semiconductors, it shifts to the center of the gap. Reproduced with permission from Ref. [19]. Copyright 2013, John Wiley & Sons.

Zha et al. investigated the O-functionalized Hf_2C and Ti_2C and proposed that at room temperature, a 5 μm-thick Hf_2CO_2 flake showed a thermal conductivity of 86.25 W m^{-1} K^{-1} in the armchair direction with a lower thermal expansion coefficient of 6.094×10^{-6} K^{-1} compared to most metals [99]. Besides, it is worth noting that the thermal conductivity of Ti_2CO_2 was lower while the carrier mobility was higher than Hf_2CO_2.

Kumar and Schwingenschlögl predicted the TE behavior of Sc_2CT_x by DFT and the Boltzmann transport formalism [100]. It was found that $Sc_2C(OH)_2$ showed the best TE performance, which is attributed to the lowest lattice thermal conductivity at intermediate temperature, despite its relatively low Seebeck coefficient.

4. Summary and outlook

In summary, recent developments of MXene-based energy storage and conversion materials and devices have been reviewed. MXenes are generally synthesized via selective etching of the A-layers from the MAX parent phase. Aside from the HF solution, other milder and less toxic etchants such as mixture of LiF with HCl or H_2SO_4 have been successfully used to extract the A element. Moreover, the hydrothermal reactions, as well as solid solution based ultransonication are effective aid for formation of particular MXenes. However, the MXenes produced by these synthetic routes are randomly functionalized by more than one termination groups, and therefore the fabrication of MXenes with a specific surface terminations is one of the major challenges. In addition, a fluoride-free synthesis strategy is of vital importance for further advances of MXenes. When appropriate molecules such as DMSO are intercalated into MXenes, large-scale delamination occurs, thereby forming single- or few-layers MXene and flexible, free-standing MXene paper.

To confirm whether MAX phase is transfered to MXene, XRD provides adequate information, while EDS can reveal the proportion of unreacted MAX. XPS and NMR have also been employed to obtain the detail of the surface termination groups, including their composition and connectivity in the MXenes. However, our current understanding for the complex surface chemistry and interlayer interaction of MXenes is still limited. Thus, both experimental characterizations and theoretical simulations remain essential to obtain a complete insight into their structures and hence guide experimental efforts to acquire MXenes with finely tuned properties.

Three major applications of MXenes for energy storage and conversion, supercapacitors, batteries and thermoelectric materials, are under thorough discussion. The 2D morphology, excellent mechanical stability and good electrical conductivities of MXenes render them fascinating electrode materials for supercapacitors and batteries. The intercalation of organic, inorganic and ionic particles into the MXenes interlayer is requisite for the applications in supercapacitor and battery. Large volumetric changes during intercalation may require MXenes layers pillaring with polymers or small molecules before using as supercapacitor electrodes. OLC, RGO, Nb_2O_5, PPy, PDDA, and PVA can comprise composites with different MXenes to serve as electrochemical capacitor electrodes, which further increase the capacitances and stabilities during cycling process. It is worth noting that the PPy/MXene composites exhibit the largest capacitance and best cycling performance so far, which opens up a promising avenue to fabricate other MXenes/polymer composites as supercapacitor electrodes. Relatively high capacities and charging/discharging stability in MXene-based LIBs have been achieved. Na^+ and some multivalent ions beyond Li^+ can be intercalated into MXene interlayers, suggesting that MXenes are also potential host materials in non-Li^+ and hybrid batteries. In fact, NIBs using MXenes with relatively large capacities have been produced and the corresponding mechanism of Na^+ intercalation and electrochemical reactions have been proposed. With respect to thermoelectric properties of MXenes, the majority of current reports are theoretical calculation and modeling. Hence, many challenges remain for experimental fabrication of outstanding MXene based thermoelectric materials and devices.

Regardless of these exciting advancements in MXenes for energy storage and conversion, much research efforts on surface engineering of MXenes, the design of device configuration, and an understanding of the mechanisms behind specific properties are urgently needed to attain desired MXenes and their composites for future applications.

Acknowledgements

Z.L. acknowledges the support of National Natural Science Foundation of China (NSFC) under grant No. 51673044.

References

[1] K.S. Novoselov, A.K. Geim, S.V. Morozov, D. Jiang, Y. Zhang, S.V. Dubonos, I.V. Grigorieva, A.A. Firsov, Electric field effect in atomically thin carbon films, Science 306 (2004) 666–669.
[2] E.P. Randviir, D.A.C. Brownson, C.E. Banks, A decade of graphene research: production, applications and outlook, Mater. Today 17 (2014) 426–432.
[3] G.R. Bhimanapati, Z. Lin, V. Meunier, Y. Jung, J. Cha, S. Das, D. Xiao, Y. Son, M.S. Strano, V.R. Cooper, L. Liang, S.G. Louie, E. Ringe, W. Zhou, S.S. Kim, R.R. Naik, B.G. Sumpter, H. Terrones, F. Xia, Y. Wang, J. Zhu, D. Akinwande, N. Alem, J.A. Schuller, R.E. Schaak, M. Terrones, J.A. Robinson, Recent advances in two-dimensional materials beyond graphene, ACS Nano 9 (2015) 11509–11539.
[4] A. Jain, Y. Shin, K.A. Persson, Computational predictions of energy materials using density functional theory, Nat. Rev. Mater 1 (2016) 1–13.
[5] M.R. Lukatskaya, B. Dunn, Y. Gogots, Multidimensional materials and device architectures for future hybrid energy storage, Nat. Commun. 7 (2016) 12647.
[6] Q. Pang, X. Liang, C.Y. Kwok, L.F. Nazar, Advances in lithium-sulfur batteries based on multifunctional cathodes and electrolytes, Nat. Energy 1 (2016) 16132.
[7] F. Feng, J. Wu, C. Wu, Y. Xie, Regulating the electrical behaviors of 2D inorganic nanomaterials for energy applications, Small 11 (2015) 654–666.
[8] L. Niu, J.N. Coleman, H. Zhang, H. Shin, M. Chhowalla, Z. Zheng, Production of two-dimensional nanomaterials via liquid-based direct exfoliation, Small 12 (2016) 272–293.
[9] M. Naguib, M. Kurtoglu, V. Presser, J. Lu, J. Niu, M. Heon, L. Hultman, Y. Gogotsi, M.W. Barsoum, Two-dimensional nanocrystals produced by exfoliation of Ti_3AlC_2, Adv. Mater 23 (2011) 4248–4253.
[10] M. Naguib, V.N. Mochalin, M.W. Barsoum, Y. Gogotsi, 25th Anniversary Article: MXenes: a new family of two-dimensional materials, Adv. Mater 26 (2014) 992–1005.
[11] J. Zhou, X. Zha, F.Y. Chen, Q. Ye, P. Eklund, S. Du, Q. Huang, A two-dimensional zirconium carbide by selective etching of Al_3C_3 from nanolaminated $Zr_3Al_3C_5$, Angew. Chem. Int. Ed. 55 (2016) 5008–5013.
[12] B. Anasori, Y. Xie, M. Beidaghi, J. Lu, B.C. Hosler, L. Hultman, P.R.C. Kent, Y. Gogotsi, M.W. Barsoum, Two-dimensional, ordered, double transition metals carbides (MXenes), ACS Nano 9 (2015) 9507–9516.
[13] M. Naguib, O. Mashtalir, J. Carle, V. Presser, J. Lu, L. Hultman, Y. Gogotsi, M.W. Barsoum, Two-dimensional transition metal carbides, ACS Nano 6 (2012) 1322–1331.
[14] M. Naguib, J. Halim, J. Lu, K.M. Cook, L. Hultman, Y. Gogotsi, M.W. Barsoum, New two-dimensional niobium and vanadium carbides as promising materials for Li-Ion batteries, J. Am. Chem. Soc. 135 (2013) 15966–15969.
[15] R. Meshkiana, L.-Å. Näslund, J. Halima, J. Lu, M.W. Barsoum, Johanna Rosen, Synthesis of two-dimensional molybdenum carbide, Mo_2C, from the gallium based atomic laminate Mo_2Ga_2C, Scr. Mater 108 (2015) 147–150.
[16] J. Yang, M. Naguib, M. Ghidiu, L.-M. Pan, J. Gu, J. Nanda, J. Halim, Y. Gogotsi, M.W. Barsoum, Two-dimensional Nb-based M_4C_3 solid solutions (MXenes), J. Am. Ceram. Soc. 99 (2016) 660–666.
[17] P. Urbankowski, B. Anasori, T. Makaryan, D. Er, S. Kota, P.L. Walsh, M. Zhao, V.B. Shenoy, M.W. Barsouma, Y. Gogotsi, Synthesis of two-dimensional titanium nitride Ti_4N_3 (MXene), Nanoscale 8 (2016) 11385–11391.
[18] R. Meshkian, Q. Tao, M. Dahlqvist, J. Lu, L. Hultman, J. Rosen, Theoretical stability and materials synthesis of a chemically ordered MAX phase, Mo_2ScAlC_2, and its two-dimensional derivate Mo_2ScC_2 MXene, Acta Mater 125 (2017) 476–480.
[19] M. Khazaei, M. Arai, T. Sasaki, C.-Y. Chung, N.S. Venkataramanan, M. Estili, Y. Sakka, Y. Kawazoe, Novel electronic and magnetic properties of two-dimensional transition metal carbides and nitrides, Adv. Funct. Mater 23 (2013) 2185–2192.

[20] V.M.H. Ng, H. Huang, K. Zhou, P.S. Lee, W. Que, J.Z. Xu, L.B. Kong, Recent progress in layered transition metal carbides and/or nitrides (MXenes) and their composites: synthesis and applications, J. Mater. Chem. A 5 (2017) 3039–3068.

[21] C. Shi, M. Beidaghi, M. Naguib, O. Mashtalir, Y. Gogotsi, S.J.L. Billinge, Structure of nanocrystalline Ti_3C_2 MXene using atomic pair distribution function, Phys. Rev. Lett. 112 (2014) 125501.

[22] H.-W. Wang, M. Naguib, K. Page, D.J. Wesolowski, Y. Gogotsi, Resolving the structure of $Ti_3C_2T_x$ MXenes through multilevel structural modeling of the atomic pair distribution function, Chem. Mater 28 (2016) 349–359.

[23] M. Ghidiu, M.R. Lukatskaya, M.-Q. Zhao, Y. Gogotsi, M.W. Barsoum, Conductive two-dimensional titanium carbide 'clay' with high volumetric capacitance, Nature 516 (2014) 78–81.

[24] J. Halim, M.R. Lukatskaya, K.M. Cook, J. Lu, C.R. Smith, L.-Å. Näslund, S.J. May, L. Hultman, Y. Gogotsi, P. Eklund, M.W. Barsoum, Transparent conductive two-dimensional titanium carbide epitaxial thin films, Chem. Mater 26 (2014) 2374–2381.

[25] M. Ashton, K. Mathew, R.G. Hennig, S.B. Sinnott, Predicted surface composition and thermodynamic stability of MXenes in solution, J. Phys. Chem. C 120 (2016) 3550–3556.

[26] X.-H. Zha, J. Yin, Y. Zhou, Q. Huang, K. Luo, J. Lang, J.S. Francisco, J. He, S. Du, Intrinsic structural, electrical, thermal, and mechanical properties of the promising conductor Mo_2C MXene, J. Phys. Chem. C 120 (2016) 15082–15088.

[27] O. Mashtalir, M. Naguib, V.N. Mochalin, Y. Dall'Agnese, M. Heon, M.W. Barsoum, Y. Gogotsi, Intercalation and delamination of layered carbides and carbonitrides, Nat. Commun. 4 (2013) 1716.

[28] M.R. Lukatskaya, O. Mashtalir, C.E. Ren, Y. Dall'Agnese, P. Rozier, P.L. Taberna, M. Naguib, P. Simon, M.W. Barsoum, Y. Gogotsi, Cation intercalation and high volumetric capacitance of two-dimensional titanium carbide, Science 341 (2013) 1502–1505.

[29] N.C. Osti, M. Naguib, A. Ostadhossein, Y. Xie, P.R.C. Kent, B. Dyatkin, G. Rother, W.T. Heller, A.C.T. van Duin, Y. Gogotsi, E. Mamontov, Effect of metal ion intercalation on the structure of MXene and water dynamics on its internal surfaces, ACS Appl. Mater. Interfaces 8 (2016) 8859–8863.

[30] Y. Zhong, X. Xia, F. Shi, J. Zhan, J. Tu, H.J. Fan, Transition metal carbides and nitrides in energy storage and conversion, Adv. Sci. 3 (2016) 1500286.

[31] L. Peng, Y. Zhu, D. Chen, R.S. Ruoff, G. Yu, Two-dimensional materials for beyond-lithium-ion batteries, Adv. Energy Mater 6 (2016) 1600025.

[32] X. Zhang, L. Hou, A. Ciesielski, P. Samorì, 2D Materials beyond graphene for high-performance energy storage applications, Adv. Energy Mater 6 (2016) 1600671.

[33] B. Mendoza-Sánchez, Y. Gogotsi, Synthesis of two-dimensional materials for capacitive energy storage, Adv. Mater 28 (2016) 6104–6135.

[34] Y. Ying, Y. Liu, X. Wang, Y. Mao, W. Cao, P. Hu, X. Peng, Two-dimensional titanium carbide for efficiently reductive removal of highly toxic chromium(VI) from water, ACS Appl. Mater. Interfaces 7 (2015) 1795–1803.

[35] L. Wang, L. Yuan, K. Chen, Y. Zhang, Q. Deng, S. Du, Q. Huang, L. Zheng, J. Zhang, Z. Chai, M.W. Barsoum, X. Wang, W. Shi, Loading actinides in multilayered structures for nuclear waste treatment: the first case study of uranium capture with vanadium carbide MXene, ACS Appl. Mater. Interfaces 8 (2016) 16396–16403.

[36] K. Rasool, M. Helal, A. Ali, C.E. Ren, Y. Gogotsi, K.A. Mahmoud, Antibacterial activity of $Ti_3C_2T_x$ MXene, ACS Nano 10 (2016) 3674–3684.

[37] C.E. Ren, K.B. Hatzell, M. Alhabeb, Z. Ling, K.A. Mahmoud, Y. Gogotsi, Charge- and size-selective ion sieving through $Ti_3C_2T_x$ MXene membranes, J. Phys. Chem. Lett. 6 (2015) 4026–4031.

[38] X.-f. Yu, Y.-c. Li, J.-b. Cheng, Z.-b. Liu, Q.-z. Li, W.-z. Li, X. Yang, B. Xiao, Monolayer Ti_2CO_2: a promising candidate for NH_3 sensor or capturer with high sensitivity and selectivity, ACS Appl. Mater. Interfaces 7 (2015) 13707–13713.

[39] H. Pan, Ultra-high electrochemical catalytic activity of MXenes, Sci. Rep. 6 (2016) 32531.

[40] Z.W. Seh, K.D. Fredrickson, B. Anasori, J. Kibsgaard, A.L. Strickler, M.R. Lukatskaya, Y. Gogotsi, T.F. Jaramillo, A. Vojvodic, Two-dimensional molybdenum carbide (MXene) as an efficient electrocatalyst for hydrogen evolution, ACS Energy Lett. 1 (2016) 589–594.

[41] J. Emmerlicha, D. Musicb, P. Eklunda, O. Wilhelmssonc, U. Janssonc, J.M. Schneiderb, H. Högberga, L. Hultman, Thermal stability of TiSiC thin films, Acta Mater 55 (2007) 1479–1488.

[42] E.N. Hoffman, G. Yushin, M.W. Barsoum, Y. Gogotsi, Synthesis of carbide-derived carbon by chlorination of Ti_2AlC, Chem. Mater 17 (2005) 2317–2322.

[43] X. Zhang, J. Xu, H. Wang, J. Zhang, H. Yan, B. Pan, J. Zhou, Y. Xie, Ultrathin nanosheets of MAX phases with enhanced thermal and mechanical properties in polymeric compositions: $Ti_3Si_{0.75}Al_{0.25}C_2$, Angew. Chem. Int. Ed. 52 (2013) 4361–4365.

[44] O. Mashtalir, M.R. Lukatskaya, M.-Q. Zhao, M.W. Barsoum, Y. Gogotsi, Amine-assisted delamination of Nb_2C MXene for Li-ion energy storage devices, Adv. Mater 27 (2015) 3501–3506.

[45] M.A. Hope, A.C. Forse, K.J. Griffith, M.R. Lukatskaya, M. Ghidiu, Y. Gogotsi, C.P. Grey, NMR reveals the surface functionalisation of Ti_3C_2 MXene, Phys. Chem. Chem. Phys. 18 (2016) 5099–5102.

[46] K. Hantanasirisakul, M.-Q. Zhao, P. Urbankowski, J. Halim, B. Anasori, S. Kota, C.E. Ren, M.W. Barsoum, Y. Gogotsi, Fabrication of $Ti_3C_2T_x$ MXene transparent thin films with tunable optoelectronic properties, Adv. Electron. Mater 2 (2016) 1600050.

[47] A.D. Dillon, M.J. Ghidiu, A.L. Krick, J. Griggs, S.J. May, Y. Gogotsi, M.W. Barsoum, A.T. Fafarman, Highly conductive optical quality solution-processed films of 2D titanium carbide, Adv. Funct. Mater 26 (2016) 4162–4168.

[48] X. Sang, Y. Xie, M.-W. Lin, M. Alhabeb, K.L.V. Aken, Y. Gogotsi, P.R.C. Kent, K. Xiao, R.R. Unocic, Atomic defects in monolayer titanium carbide ($Ti_3C_2T_x$) MXene, ACS Nano 10 (2016) 9193–9200.

[49] X. Xie, Y. Xue, L. Li, S. Chen, Y. Nie, W. Dinga, Z. Wei, Surface Al leached Ti_3AlC_2 as a substitute for carbon for use as a catalyst support in a harsh corrosive electrochemical system, Nanoscale 6 (2014) 11035–11040.

[50] L. Wang, H. Zhang, B. Wang, C. Shen, C. Zhang, Q. Hu, A. Zhou, B. Liu, Synthesis and electrochemical performance of $Ti_3C_2T_x$ with hydrothermal process, Electron. Mater. Lett. 12 (2016) 702–710.

[51] J. Halima, K.M. Cookd, M. Naguibe, P. Eklundc, Y. Gogotsia, J. Rosenc, M.W. Barsoum, X-ray photoelectron spectroscopy of select multi-layered transition metal carbides (MXenes), Appl. Surf. Sci. 362 (2016) 406–417.

[52] K.J. Harris, M. Bugnet, M. Naguib, M.W. Barsoum, G.R. Goward, Direct measurement of surface termination groups and their connectivity in the 2D MXene V_2CT_x using NMR spectroscopy, J. Phys. Chem. C 119 (2015) 13713–13720.

[53] M. Ghidiu, S. Kota, J. Halim, A.W. Sherwood, N. Nedfors, J. Rosen, V.N. Mochalin, M.W. Barsoum, Alkylammonium cation intercalation into Ti_3C_2 (MXene): effects on properties and ion-exchange capacity estimation, Chem. Mater 29 (2017) 1099–1106.

[54] M. Ghidiu, J. Halim, S. Kota, D. Bish, Y. Gogotsi, M.W. Barsoum, Ion-exchange and cation solvation reactions in Ti_3C_2 MXene, Chem. Mater 28 (2016) 3507–3514.

[55] N. Jäckel, B. Krüner, K.L.V. Aken, M. Alhabeb, B. Anasori, F. Kaasik, Y. Gogotsi, V. Presser, Electrochemical in situ tracking of volumetric changes in two-dimensional metal carbides (MXenes) in ionic liquids, ACS Appl. Mater. Interfaces 8 (2016) 32089–32093.

[56] J. Li, X. Yuan, C. Lin, Y. Yang, L. Xu, X. Du, J. Xie, J. Lin, J. Sun, Achieving high pseudocapacitance of 2D titanium carbide (MXene) by cation intercalation and surface modification, Adv. Energy Mater 7 (2017) 1602725.

[57] M.R. Lukatskaya, S.-M. Bak, X. Yu, X.-Q. Yang, M.W. Barsoum, Y. Gogotsi, Probing the mechanism of high capacitance in 2D titanium carbide using in situ X-ray absorption spectroscopy Adv, Energy Mater 5 (2015) 1500589.

[58] M. Hu, Z. Li, T. Hu, S. Zhu, C. Zhang, X. Wang, High-capacitance mechanism for $Ti_3C_2T_x$ MXene by in situ electrochemical Raman spectroscopy investigation, ACS Nano 10 (2016) 11344–11350.

[59] M.-Q. Zhao, C.E. Ren, Z. Ling, M.R. Lukatskaya, C. Zhang, K.L.V. Aken, M.W. Barsoum, Y. Gogotsi, Flexible MXene/carbon nanotube composite paper with high volumetric capacitance, Adv. Mater 27 (2015) 339–345.

[60] C. Zhao, Q. Wang, H. Zhang, S. Passerini, X. Qian, Two-dimensional titanium carbide/RGO composite for high-performance supercapacitors, ACS Appl. Mater. Interfaces 8 (2016) 15661–15667.

[61] M. Boota, B. Anasori, C. Voigt, M.-Q. Zhao, M.W. Barsoum, Y. Gogotsi, Pseudocapacitive electrodes produced by oxidant-free polymerization of pyrrole between the layers of 2D titanium carbide (MXene), Adv. Mater 28 (2016) 1517–1522.

[62] Z. Ling, C.E. Ren, M.-Q. Zhao, J. Yang, J.M. Giammarco, J. Qiuc, M.W. Barsoum, Y. Gogotsi, Flexible and conductive MXene films and nanocomposites with high capacitance, Proc. Nat. Acad. Sci. 111 (2014) 16676–16681.

[63] M. Zhu, Y. Huang, Q. Deng, J. Zhou, Z. Pei, Q. Xue, Y. Huang, Z. Wang, H. Li, Q. Huang, C. Zhi, Highly flexible, free-standing supercapacitor electrode with enhanced performance obtained by hybridizing polypyrrole chains with MXene, Adv. Energy Mater 6 (2016) 1600969.

[64] J. Luo, W. Zhang, H. Yuan, C. Jin, L. Zhang, H. Huang, C. Liang, Y. Xia, J. Zhang, Y. Gan, X. Tao, Pillared structure design of MXene with ultralarge interlayer spacing for high-performance lithium-ion capacitors, ACS Nano 11 (2017) 2459–2469.

[65] N. Kurra, B. Ahmed, Y. Gogotsi, H.N. Alshareef, MXene-on-paper coplanar microsupercapacitors, Adv. Energy Mater 6 (2016) 1601372.

[66] Y.-Y. Peng, B. Akuzum, N. Kurra, M.-Q. Zhao, M. Alhabeb, B. Anasori, E.C. Kumbur, H.N. Alshareef, M.-D. Gerc, Y. Gogotsi, All-MXene (2D titanium carbide) solid-state microsupercapacitors for on-chip energy storage, Energy Environ. Sci. 9 (2016) 2847–2854.

[67] R.B. Rakhi, B. Ahmed, M.N. Hedhili, D.H. Anjum, H.N. Alshareef, Effect of postetch annealing gas composition on the structural and electrochemical properties of Ti_2CT_x MXene electrodes for supercapacitor applications, Chem. Mater 27 (2015) 5314–5323.

[68] S. Kajiyama, L. Szabova, H. Iinuma, A. Sugahara, K. Gotoh, K. Sodeyama, Y. Tateyama, M. Okubo, A. Yamada, Enhanced Li-ion accessibility in MXene titanium carbide by steric chloride termination, Adv. Energy Mater 7 (2017) 1601873.

[69] J. Halim, S. Kota, M.R. Lukatskaya, M. Naguib, M.-Q. Zhao, E.J. Moon, J. Pitock, J. Nanda, S.J. May, Y. Gogotsi, M.W. Barsoum, Synthesis and characterization of 2D molybdenum carbide (MXene), Adv. Funct. Mater 26 (2016) 3118–3127.

[70] C. Zhang, M. Beidaghi, M. Naguib, M.R. Lukatskaya, M.-Q. Zhao, B. Dyatkin, K.M. Cook, S.J. Kim, B. Eng, X. Xiao, D. Long, W. Qiao, B. Dunn, Y. Gogotsi, Synthesis and charge storage properties of hierarchical niobium pentoxide/

carbon/niobium carbide (MXene) hybrid materials, Chem. Mater 28 (2016) 3937–3943.
[71] M. Acerce, D. Voiry, M. Chhowalla, Metallic 1T phase MoS_2 nanosheets as supercapacitor electrode materials, Nat. Nanotech 10 (2015) 313–318.
[72] J. Yan, Z. Fan, W. Sun, G. Ning, T. Wei, Q. Zhang, R. Zhang, L. Zhi, F. Wei, Advanced asymmetric supercapacitors based on $Ni(OH)_2$/graphene and porous graphene electrodes with high energy density, Adv. Funct. Mater 22 (2012) 2632–2641.
[73] H. Pan, Y.-S. Hu, L. Chen, Room-temperature stationary sodium-ion batteries for large-scale electric energy storage, Energy Environ. Sci. 6 (2013) 2338–2360.
[74] E. Yoo, J. Kim, E. Hosono, H.-s. Zhou, T. Kudo, I. Honma, Large reversible Li storage of graphene nanosheet families for use in rechargeable lithium ion batteries, Nano Lett. 8 (2008) 2277–2282.
[75] X. Cao, Y. Shi, W. Shi, X. Rui, Q. Yan, J. Kong, H. Zhang, Preparation of MoS_2-coated three-dimensional graphene networks for high-performance anode material in lithium-ion batteries, Small 9 (2013) 3433–3438.
[76] L. Chen, G. Zhou, Z. Liu, X. Ma, J. Chen, Z. Zhang, X. Ma, F. Li, H.M. Cheng, W. Ren, Scalable clean exfoliation of high-quality few-layer black phosphorus for a flexible lithium ion battery, Adv. Mater 28 (2016) 510–517.
[77] D. Er, J. Li, M. Naguib, Y. Gogotsi, V.B. Shenoy, Ti_3C_2 MXene as a high capacity electrode material for metal (Li, Na, K, Ca) ion batteries, ACS Appl. Mater. Interfaces 6 (2014) 11173–11179.
[78] M.D. Levi, M.R. Lukatskaya, S. Sigalov, M. Beidaghi, N. Shpigel, L. Daikhin, D. Aurbach, M.W. Barsoum, Y. Gogotsi, Solving the capacitive paradox of 2D MXene using electrochemical quartz-crystal admittance and in situ electronic conductance measurements, Adv. Energy Mater 5 (2015) 1400815.
[79] D. Sun, Q. Hu, J. Chen, X. Zhang, L. Wang, Q. Wu, A. Zhou, Structural transformation of MXene (V_2C, Cr_2C, and Ta_2C) with O Groups during lithiation: a first-principles investigation, ACS Appl. Mater. Interfaces 8 (2016) 74–81.
[80] J. Come, Y. Xie, M. Naguib, S. Jesse, S.V. Kalinin, Y. Gogotsi, P.R.C. Kent, N. Balke, Nanoscale elastic changes in 2D $Ti_3C_2T_x$ (MXene) pseudocapacitive electrodes, Adv. Energy Mater 6 (2016) 1502290.
[81] J. Luo, X. Tao, J. Zhang, Y. Xia, H. Huang, L. Zhang, Y. Gan, C. Liang, W. Zhang, Sn^{4+} ion decorated highly conductive Ti_3C_2 MXene: promising lithium-ion anodes with enhanced volumetric capacity and cyclic performance, ACS Nano 10 (2016) 2491–2499.
[82] G. Zou, Z. Zhang, J. Guo, B. Liu, Q. Zhang, C. Fernandez, Q. Peng, Synthesis of MXene/Ag composites for extraordinary long cycle lifetime lithium storage at high rates, ACS Appl. Mater. Interfaces 8 (2016) 22280–22286.
[83] A.T. Tesfaye, O. Mashtalir, M. Naguib, M.W. Barsoum, Y. Gogotsi, T. Djenizian, Anodized Ti_3SiC_2 as an anode material for Li-ion microbatteries, ACS Appl. Mater. Interfaces 8 (2016) 16670–16676.
[84] C.J. Zhang, S.J. Kim, M. Ghidiu, M.-Q. Zhao, M.W. Barsoum, V. Nicolosi, Y. Gogotsi, Layered orthorhombic Nb_2O_5@$Nb_4C_3T_x$ and TiO_2@$Ti_3C_2T_x$ hierarchical composites for high performance Li-ion batteries, Adv. Funct. Mater 26 (2016) 4143–4151.
[85] Q. Sun, Y. Dai, Y. Ma, T. Jing, W. Wei, B. Huang, Ab initio prediction and characterization of Mo_2C monolayer as anodes for lithium-ion and sodium-ion batteries, J. Phys. Chem. Lett. 7 (2016) 937–943.
[86] M. Ashton, R.G. Hennig, S.B. Sinnott, Computational characterization of lightweight multilayer MXene Li-ion battery anodes, Appl. Phys. Lett. 108 (2016) 023901.
[87] H.-J. Peng, Q. Zhang, Designing host materials for sulfur cathodes: from physical confinement to surface chemistry, Angew. Chem. Int. Ed. 54 (2015) 11018–11020.
[88] X. Liang, A. Garsuch, L.F. Nazar, Sulfur cathodes based on conductive MXene nanosheets for high performance lithium-sulfur batteries, Angew. Chem. Int. Ed. 127 (2015) 3979–3983.
[89] A. Byeon, M.-Q. Zhao, C.E. Ren, J. Halim, S. Kota, P. Urbankowski, B. Anasori, M.W. Barsoum, Y. Gogotsi, Two-dimensional titanium carbide MXene as a cathode material for hybrid magnesium/lithium-ion batteries, ACS Appl. Mater. Interfaces 9 (2017) 4296–4300.
[90] Y. Xie, Y. Dall'Agnese, M. Naguib, Y. Gogotsi, M.W. Barsoum, H.L. Zhuang, P.R.C. Kent, Prediction and characterization of MXene nanosheet anodes for non-lithium-ion batteries, ACS Nano 8 (2014) 9606–9615.
[91] C. Eames, M.S. Islam, Ion intercalation into two-dimensional transition-metal carbides: global screening for new high-capacity battery materials, J. Am. Chem. Soc. 136 (2014) 16270–16276.
[92] Y.-X. Yu, Prediction of mobility, enhanced storage capacity, and volume change during sodiation on interlayer-expanded functionalized Ti_3C_2 MXene anode materials for sodium-ion batteries, J. Phys. Chem. C 120 (2016) 5288–5296.
[93] S. Kajiyama, L. Szabova, K. Sodeyama, H. Iinuma, Ryohei Morita, K. Gotoh, Y. Tateyama, M. Okubo, A. Yamada, Sodium-ion intercalation mechanism in MXene nanosheets, ACS Nano 10 (2016) 3334–3341.
[94] X. Wang, S. Kajiyama, H. Iinuma, E. Hosono, S. Oro, I. Moriguchi, M. Okubo, A. Yamada, Pseudocapacitance of MXene nanosheets for high-power sodium-ion hybrid capacitors, Nat. Commun. 6 (2015) 6544.
[95] Y. Dall'Agnese, P.-L. Taberna, Y. Gogotsi, P. Simon, Two-dimensional vanadium carbide (MXene) as positive electrode for sodium-ion capacitors, J. Phys. Chem. Lett. 6 (2015) 2305–2309.
[96] J. Sun, H.W. Lee, M. Pasta, H. Yuan, G. Zheng, Y. Sun, Y. Li, Y. Cui, A phosphorene-graphene hybrid material as a high-capacity anode for sodium-ion batteries, Nat. Nanotech 10 (2015) 980–985.
[97] M. Khazaei, M. Arai, T. Sasaki, M. Estilic, Y. Sakka, Two-dimensional molybdenum carbides: potential thermoelectric materials of the MXene family, Phys. Chem. Chem. Phys. 16 (2014) 7841–7849.
[98] A.N. Gandi, H.N. Alshareef, U. Schwingenschlögl, Thermoelectric performance of the MXenes M_2CO_2 (M = Ti, Zr, or Hf), Chem. Mater 28 (2016) 1647–1652.
[99] X.-H. Zha, Q. Huang, J. He, H. He, J. Zhai, J.S. Francisco, S. Du, The thermal and electrical properties of the promising semiconductor MXene Hf_2CO_2, Sci. Rep. 6 (2016) 27971.
[100] S. Kumar, U. Schwingenschlögl, Thermoelectric performance of functionalized Sc_2C MXenes, Phys. Rev. B 94 (2016) 035405.